

1 **Approximate analysis of three-dimensional groundwater flow toward a**
2 **radial collector well in a finite-extent unconfined aquifer**

3 **Ching-Sheng Huang¹, Jyun-Jie Chen¹, and Hund-Der Yeh^{1*}**

4
5
6
7
8 **Submitted to *Hydrology and Earth System Sciences* on June 14, 2015**

9 **Re-submitted to *Hydrology and Earth System Sciences* on July 22, 2015**

10 **Re-re-submitted to *Hydrology and Earth System Sciences* on October 14, 2015**

11 **Re-re-re-submitted to *Hydrology and Earth System Sciences* on December 18, 2015**

12
13 ¹ Institute of Environmental Engineering, National Chiao Tung University, Hsinchu, Taiwan.

14
15 *** Corresponding Author**

16 Address: Institute of Environmental Engineering, National Chiao Tung University, 1001

17 University Road, Hsinchu 300, Taiwan

18 E-mail address: hdyeh@mail.nctu.edu.tw; Tel: 886-3-5731910; Fax: 886-3-5725958

19 **Abstract**

20 This study develops a three-dimensional mathematical model for describing transient
21 hydraulic head distributions due to pumping at a radial collector well (RCW) in a rectangular
22 confined or unconfined aquifer bounded by two parallel streams and no-flow boundaries. The
23 streams with low-permeability streambeds fully penetrate the aquifer. The governing equation
24 with a point-sink term is employed. A first-order free surface equation delineating the water
25 table decline induced by the well is considered. Robin boundary conditions are adopted to
26 describe fluxes across the streambeds. The head solution for the point sink is derived by
27 applying the methods of finite integral transform and Laplace transform. The head solution for
28 a RCW is obtained by integrating the point-sink solution along the laterals of the RCW and
29 then dividing the integration result by the sum of lateral lengths. On the basis of Darcy's law
30 and head distributions along the streams, the solution for the stream depletion rate (SDR) can
31 also be developed. With the aid of the head and SDR solutions, the sensitivity analysis can then
32 be performed to explore the response of the hydraulic head to the change in a specific parameter
33 such as the horizontal and vertical hydraulic conductivities, streambed permeability, specific
34 storage, specific yield, lateral length and well depth. Spatial head distributions subject to the
35 anisotropy of aquifer hydraulic conductivities are analyzed. A quantitative criterion is provided
36 to identify whether groundwater flow at a specific region is 3-D or 2-D without the vertical
37 component. In addition, another criterion is also given to allow the neglect of vertical flow
38 effect on SDR. Conventional 2-D flow models can be used to provide accurate head and SDR
39 predictions if satisfying these two criteria.

40 **Keywords:** Robin boundary condition, sensitivity analysis, stream depletion rate, first-order
41 free surface equation, analytical solution

42 **1. Introduction**

43 The applications of a radial collector well (RCW) have received much attention in the
44 aspects of water resource supply and groundwater remediation since rapid advances in drilling
45 technology. An average yield for the well approximates 27,000 m³/day (Todd and Mays, 2005).
46 As compared to vertical wells, RCWs require less operating cost, produce smaller drawdown,
47 and have better efficiency of withdrawing water from thin aquifers. In addition, RCWs can
48 extract water from an aquifer underlying obstacles such as buildings, but vertical wells cannot.
49 Recently, Huang et al. (2012) reviewed semi-analytical and analytical solutions associated with
50 RCWs. Since then, Yeh and Chang (2013) provided a valuable overview of articles associated
51 with RCWs.

52 A variety of analytical models involving a horizontal well, a specific case of a RCW with
53 a single lateral, in aquifers were developed (e.g., Park and Zhan, 2003; Hunt, 2005; Anderson,
54 2013). The flux along the well screen is commonly assumed to be uniform. The equation
55 describing three-dimensional (3-D) flow is used. Kawecki (2000) developed analytical
56 solutions of the hydraulic heads for the early linear flow perpendicular to a horizontal well and
57 late pseudo-radial flow toward the middle of the well in confined aquifers. They also developed
58 an approximate solution for unconfined aquifers on the basis of the head solution and an
59 unconfined flow modification. The applicability of the approximate solution was later
60 evaluated in comparison with a finite difference solution developed by Kawecki and Al-
61 Subaikhy (2005). Zhan et al. (2001) presented an analytical solution for drawdown induced by
62 a horizontal well in confined aquifers and compared the difference in the type curves based on
63 the well and a vertical well. Zhan and Zlotnik (2002) developed a semi-analytical solution of
64 drawdown due to pumping from a nonvertical well in an unconfined aquifer accounting for the
65 effect of instantaneous drainage or delayed yield when the free surface declines. They discussed
66 the influences of the length, depth, and inclination of the well on temporal drawdown

67 distributions. Park and Zhan (2002) developed a semi-analytical drawdown solution
68 considering the effects of a finite diameter, the wellbore storage, and a skin zone around a
69 horizontal well in anisotropic leaky aquifers. They found that those effects cause significant
70 change in drawdown at an early pumping period. Zhan and Park (2003) provided a general
71 semi-analytical solution for pumping-induced drawdown in a confined aquifer, an unconfined
72 aquifer on a leaky bottom, or a leaky aquifer below a water reservoir. Temporal drawdown
73 distributions subject to the aquitard storage effect were compared with those without that effect.
74 Sun and Zhan (2006) derived a semi-analytical solution of drawdown due to pumping at a
75 horizontal well in a leaky aquifer. A transient one-dimensional flow equation describing the
76 vertical flow across the aquitard was considered. The derived solution was used to evaluate the
77 Zhan and Park (2003) solution which assumed steady-state vertical flow in the aquitard.

78 Sophisticated numerical models involved in RCWs or horizontal wells were also reported.
79 Steward (1999) applied the analytic element method to approximate 3-D steady-state flow
80 induced by horizontal wells in contaminated aquifers. They discussed the relation between a
81 pumping rate and the size of a polluted area. Chen et al. (2003) utilized the polygon finite
82 difference method to deal with three kinds of seepage-pipe flows including laminar, turbulent,
83 and transitional flows within a finite-diameter horizontal well. A sandbox experiment was also
84 carried out to verify the prediction made by the method. Mohamad and Rushton (2006) used
85 MODFLOW to predict flows inside an aquifer, from the aquifer to a horizontal well, and within
86 the well. The predicted head distributions were compared with field data measured in Sarawak,
87 Malaysia. Su et al. (2007) used software TOUGH2 based on the integrated finite difference
88 method to handle irregular configurations of several laterals of two RCWs installed beside the
89 Russian River, Forestville, California and analyzed pumping-induced unsaturated regions
90 beneath the river. Lee et al. (2012) developed a finite element solution with triangle elements
91 to assess whether the operation of a RCW near Nakdong River in South Korea can induce

92 riverbank filtration. They concluded that the well can be used for sustainable water supply at
93 the study site. In addition, Rushton and Brassington (2013a) extended Mohamad and Rushton
94 (2006) study by enhancing the Darcy-Weisbach formula to describe frictional head lose inside
95 a horizontal well. The spatial distributions of predicted flux along the well revealed that the
96 flux at the pumping end is four times of the magnitude of that at the far end. Later, Rushton
97 and Brassington (2013b) applied the same model to a field experiment at the Seton Coast,
98 northwest England.

99 Well pumping in aquifers near streams may cause groundwater–surface water interactions
100 (e.g., Rodriguez et al., 2013; Chen et al., 2013; Zhou et al., 2013; Exner-Kittridge et al., 2014;
101 Flipo et al., 2014; Unland et al., 2014). The stream depletion rate (SDR), commonly used to
102 quantify stream water filtration into the adjacent aquifer, is defined as the ratio of the filtration
103 rate to a pumping rate. The SDR ranges from zero to a certain value which could be equal to
104 or less than unity (Zlotnik, 2004). Tsou et al. (2010) developed an analytical solution of SDR
105 for a slanted well in confined aquifers adjacent to a stream treated as a constant-head boundary.
106 They indicated that a horizontal well parallel to the stream induces the steady-state SDR of
107 unity more quickly than a slanted well. Huang et al. (2011) developed an analytical SDR
108 solution for a horizontal well in unconfined aquifers near a stream regarded as a constant-head
109 boundary. Huang et al. (2012) provided an analytical solution for SDR induced by a RCW in
110 unconfined aquifers adjacent to a stream with a low-permeability streambed under the Robin
111 condition. The influence of the configuration of the laterals on temporal SDR and spatial
112 drawdown distributions was analyzed. Recently, Huang et al. (2014) gave an exhaustive review
113 on analytical and semi-analytical SDR solutions and classified these solutions into two
114 categories. One group involved two-dimensional (2-D) flow toward a fully-penetrating vertical
115 well according to aquifer types and stream treatments. The other group included the solutions
116 involving 3-D and quasi 3-D flows in the lights of aquifer types, well types, and stream

117 treatments.

118 At present, existing analytical solutions associated with flow toward a RCW in unconfined
119 aquifers have involved laborious calculation (Huang et al., 2012) and predicted approximate
120 results (Hantush and Papadopoulos, 1962). The Huang et al. (2012) solution involves numerical
121 integration of a triple integral in predicting the hydraulic head and a quintuple integral in
122 predicting SDR. The integrand is expressed in terms of an infinite series expanded by roots of
123 nonlinear equations. The integration variables are related to those roots. The application of
124 their solution is therefore limited to those who are familiar with numerical methods. In addition,
125 the accuracy of the Hantush and Papadopoulos (1962) solution is limited to some parts of a
126 pumping period; that is, it gives accurate drawdown predictions at early and late times but
127 divergent ones at middle time.

128 The objective of this study is to present new analytical solutions of the head and SDR,
129 which overcome the above-mentioned limitations, for 3-D flow toward a RCW. A
130 mathematical model is built to describe 3-D spatiotemporal hydraulic head distributions in a
131 rectangular unconfined aquifer bounded by two parallel streams and by the no-flow stratums
132 in the other two sides. The flux across the well screen is assumed to be uniform along each of
133 the laterals. The assumption is valid for a short lateral within 150 m verified by agreement on
134 drawdown observed in field experiments and predicted by existing analytical solutions (Huang
135 et al., 2011; 2012). The streams fully penetrate the aquifer and connect the aquifer with low-
136 permeability streambeds. The model for the aquifer system with two parallel streams can be
137 used to determine the fraction of water filtration from the streams and solve the associated
138 water right problem (Sun and Zhan, 2007). The transient 3-D groundwater flow equation with
139 a point-sink term is considered. The first-order free surface equation is used to describe water
140 table decline due to pumping. Robin boundary conditions are adopted to describe fluxes across
141 the streambeds. The head solution for a point sink is derived by the methods of Laplace

142 transform and finite integral transform. The analytical head solution for a RCW is then obtained
143 by integrating the point-sink solution along the well and dividing the integration result by the
144 total lateral length. The RCW head solution is expressed in terms of a triple series expanded
145 by eigenvalues which can be obtained by a numerical algorithm such as Newton's method. On
146 the basis of Darcy's law and the RCW head solution, the SDR solution can then be obtained in
147 terms of a double series with fast convergence. With the aid of both solutions, the sensitivity
148 analysis is performed to investigate the response of the hydraulic head to the change in each of
149 aquifer parameters. Spatial head distributions subject to the anisotropy of aquifer hydraulic
150 conductivities are analyzed. The influences of the vertical flow and well depth on temporal
151 SDR distributions are investigated. Moreover, temporal SDR distributions induced by a RCW
152 and a fully penetrating vertical well in confined aquifers are also compared. A quantitative
153 criterion is provided to identify whether groundwater flow at a specific region is 3-D or 2-D
154 without the vertical component. In addition, another criterion is also given to judge the
155 suitability of neglecting the vertical flow effect on SDR.

156

157 **2. Methodology**

158 **2.1. Mathematical model**

159 Consider a RCW in a rectangular unconfined aquifer bounded by two parallel streams and
160 no-flow stratum as illustrated in Figure 1. The symbols for variables and parameters are
161 defined in Table 1. The origin of the Cartesian coordinate is located at the lower left corner.
162 The aquifer domain falls in the range of $0 \leq x \leq w_x$, $0 \leq y \leq w_y$, and $-H \leq z \leq 0$. The
163 RCW consists of a caisson and several laterals, each of which extends with length L_k and
164 counterclockwise with angle θ_k where $k \in 1, 2, \dots, N$ and N is the number of laterals. The
165 caisson is located at (x_0, y_0) , and the surrounding laterals are at $z = -z_0$.

166 First of all, a mathematical model describing 3-D flow toward a point sink in the aquifer

167 is proposed. The equation describing 3-D hydraulic head distribution $h(x, y, z, t)$ is expressed
 168 as

$$169 \quad K_x \frac{\partial^2 h}{\partial x^2} + K_y \frac{\partial^2 h}{\partial y^2} + K_z \frac{\partial^2 h}{\partial z^2} = S_s \frac{\partial h}{\partial t} + Q \delta(x - x'_0) \delta(y - y'_0) \delta(z + z'_0) \quad (1)$$

170 where $\delta(\)$ is the Dirac delta function, the second term on the right-hand side (RHS) indicates
 171 the point sink, and Q is positive for pumping and negative for injection. The first term on the
 172 RHS of Eq. (1) depicts aquifer storage release based on the concept of effective stress proposed
 173 by Terzaghi (see, for example, Bear, 1979; Charbeneau, 2000), which is valid under the
 174 assumption of constant total stress. By choosing water table as a reference datum where the
 175 elevation head is set to zero, the initial condition can therefore be denoted as

$$176 \quad h = 0 \quad \text{at} \quad t = 0 \quad (2)$$

177 Note that equation (2) introduces negative hydraulic head for pumping, and the absolute value
 178 of the head equals drawdown.

179 The aquifer boundaries at $x = 0$ and $x = w_x$ are considered to be impermeable and thus
 180 expressed as

$$181 \quad \partial h / \partial x = 0 \quad \text{at} \quad x = 0 \quad (3)$$

182 and

$$183 \quad \partial h / \partial x = 0 \quad \text{at} \quad x = w_x \quad (4)$$

184 Streambed permeability is usually less than the adjacent aquifer formation. The fluxes across
 185 the streambeds can be described by Robin boundary conditions as

$$186 \quad K_y \frac{\partial h}{\partial y} - \frac{K_1}{b_1} h = 0 \quad \text{at} \quad y = 0 \quad (5)$$

187 and

$$188 \quad K_y \frac{\partial h}{\partial y} + \frac{K_2}{b_2} h = 0 \quad \text{at} \quad y = w_y \quad (6)$$

189 The free surface equation describing water table decline is written as

190
$$K_x \left(\frac{\partial h}{\partial x} \right)^2 + K_y \left(\frac{\partial h}{\partial y} \right)^2 + K_z \left(\frac{\partial h}{\partial z} \right)^2 - K_z \frac{\partial h}{\partial z} = S_y \frac{\partial h}{\partial t} \quad \text{at } z = h \quad (7)$$

191 Neuman (1972) indicated that the effect of the second-order terms in Eq. (7) is generally
 192 ignorable to develop analytical solutions. Eq. (7) is thus linearized by neglecting the quadratic
 193 terms, and the position of the water table is fixed at the initial condition (i.e., $z = 0$). The result
 194 is written as

195
$$K_z \frac{\partial h}{\partial z} = -S_y \frac{\partial h}{\partial t} \quad \text{at } z = 0 \quad (8)$$

196 Notice that Eq. (8) is applicable when the conditions $|h|/H \leq 0.1$ and $|\partial h / \partial x| +$
 197 $|\partial h / \partial y| \leq 0.01$ are satisfied. These two conditions had been studied and verified by
 198 simulations in, for example, Nyholm et al. (2002), Goldscheider and Drew (2007) and Yeh et
 199 al. (2010). Nyholm et al. (2002) achieved agreement on drawdown measured in a field pumping
 200 test and predicted by MODFLOW which models flow in the study site as confined behavior
 201 because of $|h|/H \leq 0.1$ in the pumping well. Goldscheider and Drew (2007) revealed that
 202 pumping drawdown predicted by Neuman (1972) analytical solution based on Eq. (8) agrees
 203 well with that obtained in a field pumping test. In addition, Yeh et al. (2010) also achieved
 204 agreement on the hydraulic head predicted by their analytical solution based on Eq. (8), their
 205 finite difference solution based on Eq. (7) with $\partial h / \partial y = 0$ (referring to Eq. (7a)), and Teo et
 206 al. (2003) solution derived by applying the perturbation technique to deal with Eq. (7a) when
 207 $|h|/H = 0.1$ and $|\partial h / \partial x| = 0.01$ (i.e., $\alpha = 0.1$ and $|\partial \phi / \partial x| = 0.01$ at $x = 0$ in Yeh et al.
 208 (2010, Fig. 5(a)). On the other hand, the bottom of the aquifer is considered as a no-flow
 209 boundary condition denoted as

210
$$\partial h / \partial z = 0 \quad \text{at } z = -H \quad (9)$$

211 Define dimensionless variables as $\bar{h} = (K_y H h) / Q$, $\bar{t} = (K_y t) / (S_y y_0^2)$, $\bar{x} = x / y_0$,
 212 $\bar{y} = y / y_0$, $\bar{z} = z / H$, $\bar{x}'_0 = x'_0 / y_0$, $\bar{y}'_0 = y'_0 / y_0$, $\bar{z}'_0 = z'_0 / H$, $\bar{w}_x = w_x / y_0$ and $\bar{w}_y =$

213 w_y/y_0 where the overbar denotes a dimensionless symbol, H is the initial aquifer thickness,
 214 and y_0 is a distance between stream 1 and the center of the RCW. On the basis of the
 215 definitions, Eq. (1) can be written as

$$216 \quad \kappa_x \frac{\partial^2 \bar{h}}{\partial \bar{x}^2} + \frac{\partial^2 \bar{h}}{\partial \bar{y}^2} + \kappa_z \frac{\partial^2 \bar{h}}{\partial \bar{z}^2} = \frac{\partial \bar{h}}{\partial \bar{t}} + \delta(\bar{x} - \bar{x}_0) \delta(\bar{y}' - \bar{y}'_0) \delta(\bar{z} + \bar{z}'_0) \quad (10)$$

217 where $\kappa_x = K_x/K_y$ and $\kappa_z = (K_z y_0^2)/(K_y H^2)$.

218 Similarly, the initial and boundary conditions are expressed as

$$219 \quad \bar{h} = 0 \quad \text{at} \quad \bar{t} = 0 \quad (11)$$

$$220 \quad \partial \bar{h} / \partial \bar{x} = 0 \quad \text{at} \quad \bar{x} = 0 \quad (12)$$

$$221 \quad \partial \bar{h} / \partial \bar{x} = 0 \quad \text{at} \quad \bar{x} = \bar{w}_x \quad (13)$$

$$222 \quad \partial \bar{h} / \partial \bar{y} - \kappa_1 \bar{h} = 0 \quad \text{at} \quad \bar{y} = 0 \quad (14)$$

$$223 \quad \partial \bar{h} / \partial \bar{y} + \kappa_2 \bar{h} = 0 \quad \text{at} \quad \bar{y} = \bar{w}_y \quad (15)$$

$$224 \quad \frac{\partial \bar{h}}{\partial \bar{z}} = -\frac{\gamma}{\kappa_z} \frac{\partial \bar{h}}{\partial \bar{t}} \quad \text{at} \quad \bar{z} = 0 \quad (16)$$

225 and

$$226 \quad \partial \bar{h} / \partial \bar{z} = 0 \quad \text{at} \quad \bar{z} = -1 \quad (17)$$

227 where $\kappa_1 = (K_1 y_0)/(K_y b_1)$, $\kappa_2 = (K_2 y_0)/(K_y b_2)$ and $\gamma = S_y/(S_s H)$.

228 **2.2 Head solution for point sink**

229 The model, Eqs. (10) – (17), reduces to an ordinary differential equation (ODE) with two
 230 boundary conditions in terms of \bar{z} after taking Laplace transform and finite integral transform.

231 The former transform converts $\bar{h}(\bar{x}, \bar{y}, \bar{z}, \bar{t})$ into $\hat{h}(\bar{x}, \bar{y}, \bar{z}, p)$, $\delta(\bar{x} - \bar{x}'_0) \delta(\bar{y} - \bar{y}'_0) \delta(\bar{z} - \bar{z}'_0)$

232 in Eq. (10) into $\delta(\bar{x} - \bar{x}'_0) \delta(\bar{y} - \bar{y}'_0) \delta(\bar{z} - \bar{z}'_0)/p$, and $\partial \bar{h} / \partial \bar{t}$ in Eqs. (10) and (16) into

233 $p \hat{h} - \bar{h}|_{\bar{t}=0}$ where p is the Laplace parameter, and the second term, initial condition in Eq. (11),

234 equals zero (Kreyszig, 1999). The transformed model becomes a boundary value problem

235 written as

$$236 \quad \kappa_x \frac{\partial^2 \hat{h}}{\partial \bar{x}^2} + \frac{\partial^2 \hat{h}}{\partial \bar{y}^2} + \kappa_z \frac{\partial^2 \hat{h}}{\partial \bar{z}^2} = p \hat{h} + \delta(\bar{x} - \bar{x}') \delta(\bar{y}' - \bar{y}') \delta(\bar{z} + \bar{z}') / p \quad (18)$$

237 with boundary conditions $\partial \hat{h} / \partial \bar{x} = 0$ at $\bar{x} = 0$ and $\bar{x} = \bar{w}_x$, $\partial \hat{h} / \partial \bar{y} - \kappa_1 \hat{h} = 0$ at $\bar{y} = 0$,

238 $\partial \hat{h} / \partial \bar{y} + \kappa_2 \hat{h} = 0$ at $\bar{y} = \bar{w}_y$, $\partial \hat{h} / \partial \bar{z} = -p \gamma \hat{h} / \kappa_z$ at $\bar{z} = 0$ and $\partial \hat{h} / \partial \bar{z} = 0$ at $\bar{z} = -1$.

239 We then apply finite integral transform to the problem. One can refer to Appendix A for its

240 detailed definition. The transform converts $\hat{h}(\bar{x}, \bar{y}, \bar{z}, p)$ in the problem into $\tilde{h}(\alpha_m, \beta_n, \bar{z}, p)$,

241 and $\delta(\bar{x} - \bar{x}') \delta(\bar{y} - \bar{y}')$ in Eq. (18) into $\cos(\alpha_m \bar{x}') K(\bar{y}_0')$ and $\kappa_x \partial^2 \hat{h} / \partial \bar{x}^2 + \partial^2 \hat{h} / \partial \bar{y}^2$

242 in Eq. (18) into $-(\kappa_x \alpha_m^2 + \beta_n^2) \tilde{h}$ where $(m, n) \in 1, 2, 3, \dots, \infty$, $\alpha_m = m \pi / \bar{w}_x$, $K(\bar{y}_0')$ is

243 defined in Eq. (A2) with $\bar{y} = \bar{y}_0'$, and β_n represents eigenvalues equaling the roots of the

244 following equation as (Latinopoulos, 1985)

$$245 \quad \tan(\beta_n \bar{w}_y) = \frac{\beta_n (\kappa_1 + \kappa_2)}{\beta_n^2 - \kappa_1 \kappa_2} \quad (19)$$

246 The method to determine the roots is discussed in section 2.3. In turn, Eq. (18) becomes a

247 second-order ODE defined by

$$248 \quad \kappa_z \frac{\partial^2 \tilde{h}}{\partial \bar{z}^2} - (\kappa_x \alpha_m^2 + \beta_n^2 + p) \tilde{h} = \cos(\alpha_m \bar{x}') K(\bar{y}_0') \delta(\bar{z} + \bar{z}') / p \quad (20)$$

249 with two boundary conditions denoted as

$$250 \quad \frac{\partial \tilde{h}}{\partial \bar{z}} = -\frac{p \gamma}{\kappa_z} \tilde{h} \quad \text{at} \quad \bar{z} = 0 \quad (21)$$

251 and

$$252 \quad \partial \tilde{h} / \partial \bar{z} = 0 \quad \text{at} \quad \bar{z} = -1 \quad (22)$$

253 Eq. (20) can be separated into two homogeneous ODEs as

$$254 \quad \kappa_z \frac{\partial^2 \tilde{h}_a}{\partial \bar{z}^2} - (\kappa_x \alpha_m^2 + \beta_n^2 + p) \tilde{h}_a = 0 \quad \text{for} \quad -\bar{z}' \leq \bar{z} \leq 0 \quad (23)$$

255 and

$$256 \quad \kappa_z \frac{\partial^2 \tilde{h}_b}{\partial \bar{z}^2} - (\kappa_x \alpha_m^2 + \beta_n^2 + p) \tilde{h}_b = 0 \quad \text{for} \quad -1 \leq \bar{z} \leq -\bar{z}'_0 \quad (24)$$

257 where h_a and h_b , respectively, represent the heads above and below $\bar{z} = -\bar{z}'_0$ where the point
 258 sink is located. Two continuity requirements should be imposed at $\bar{z} = -\bar{z}'_0$. The first is the
 259 continuity of the hydraulic head denoted as

$$260 \quad \tilde{h}_a = \tilde{h}_b \quad \text{at} \quad \bar{z} = -\bar{z}'_0 \quad (25)$$

261 The second describes the discontinuity of the flux due to point pumping represented by the
 262 Dirac delta function in Eq. (20). It can be derived by integrating Eq. (20) from $\bar{z} = -\bar{z}'_0^-$ to
 263 $\bar{z} = -\bar{z}'_0^+$ as

$$264 \quad \frac{\partial \tilde{h}_a}{\partial \bar{z}} - \frac{\partial \tilde{h}_b}{\partial \bar{z}} = \frac{\cos(\alpha_m \bar{x}'_0) K(\bar{y}'_0)}{p \kappa_z} \quad \text{at} \quad \bar{z} = -\bar{z}'_0 \quad (26)$$

265 Solving Eqs. (23) and (24) simultaneously with Eqs. (21), (22), (25), and (26) yields the
 266 Laplace-domain head solution as

$$267 \quad \tilde{h}_a(\alpha_m, \beta_n, \bar{z}, p) = \Omega(-\bar{z}'_0, \bar{z}, 1) \quad \text{for} \quad -\bar{z}'_0 \leq \bar{z} \leq 0 \quad (27a)$$

268 and

$$269 \quad \tilde{h}_b(\alpha_m, \beta_n, \bar{z}, p) = \Omega(\bar{z}, \bar{z}'_0, -1) \quad \text{for} \quad -1 \leq \bar{z} \leq -\bar{z}'_0 \quad (27b)$$

270 with

$$271 \quad \Omega(a, b, c) = \frac{\cosh[(1+a)\lambda] [-\kappa_z \lambda \cosh(b\lambda) + c p \gamma \sinh(b\lambda)] \cos(\alpha_m \bar{x}'_0) K(\bar{y}'_0)}{p \kappa_z \lambda (p \gamma \cosh \lambda + \kappa_z \lambda \sinh \lambda)} \quad (28)$$

$$272 \quad \lambda = \sqrt{(\kappa_x \alpha_m^2 + \beta_n^2 + p) / \kappa_z} \quad (29)$$

273 where a , b , and c are arguments. Taking the inverse Laplace transform and finite integral
 274 transform to Eq. (28) results in Eq. (31). One is referred to Appendix B for the detailed
 275 derivation. A time-domain head solution for a point sink is therefore written as

$$276 \quad \bar{h}(\bar{x}, \bar{y}, \bar{z}, \bar{t}) = \begin{cases} \Phi(-\bar{z}'_0, \bar{z}, 1) & \text{for} \quad -\bar{z}'_0 \leq \bar{z} \leq 0 \\ \Phi(\bar{z}, \bar{z}'_0, -1) & \text{for} \quad -1 \leq \bar{z} \leq -\bar{z}'_0 \end{cases} \quad (30)$$

277 with

$$278 \quad \Phi(a, b, c) = \frac{2}{\bar{w}_x} \left\{ \sum_{n=1}^{\infty} [\phi_n X_n + 2 \sum_{m=1}^{\infty} \phi_{m,n} X_{m,n} \cos(\alpha_m \bar{x})] Y_n \right\} \quad (31)$$

$$279 \quad \phi_{m,n} = \psi_{m,n} + \psi_{m,n,0} + \sum_{i=1}^{\infty} \psi_{m,n,i} \quad (32)$$

$$280 \quad \psi_{m,n} = -\cosh[(1+a)\lambda_s] \cosh(b\lambda_s) / (\kappa_z \lambda_s \sinh \lambda_s) \quad (33)$$

$$281 \quad \psi_{m,n,0} = \mu_{m,n,0} \cosh[(1+a)\lambda_0] [-\kappa_z \lambda_0 \cosh(b\lambda_0) + c p_0 \gamma \sinh(b\lambda_0)] \quad (34)$$

$$282 \quad \psi_{m,n,i} = \nu_{m,n,i} \cos[(1+a)\lambda_i] [-\kappa_z \lambda_i \cos(b\lambda_i) + c p_i \gamma \sin(b\lambda_i)] \quad (35)$$

$$283 \quad \mu_{m,n,0} = 2 \exp(p_0 \bar{t}) / \{p_0 [(1+2\gamma) \kappa_z \lambda_0 \cosh \lambda_0 + (p_0 \gamma + \kappa_z) \sinh \lambda_0]\} \quad (36)$$

$$284 \quad \nu_{m,n,i} = 2 \exp(p_i \bar{t}) / \{p_i [(1+2\gamma) \kappa_z \lambda_i \cos \lambda_i + (p_i \gamma + \kappa_z) \sin \lambda_i]\} \quad (37)$$

$$285 \quad Y_n = \frac{\beta_n \cos(\beta_n \bar{y}) + \kappa_1 \sin(\beta_n \bar{y})}{(\beta_n^2 + \kappa_1^2) [\bar{w}_y + \kappa_2 / (\beta_n^2 + \kappa_2^2)] + \kappa_1} \quad (38)$$

286 and

$$287 \quad X_{m,n} = \cos(\alpha_m \bar{x}'_0) [\beta_n \cos(\beta_n \bar{y}'_0) + \kappa_1 \sin(\beta_n \bar{y}'_0)] \quad (39)$$

288 where $\lambda_s = \sqrt{(\kappa_x \alpha_m^2 + \beta_n^2) / \kappa_z}$, $p_0 = \kappa_z \lambda_0^2 - \kappa_x \alpha_m^2 - \beta_n^2$, $p_i = -\kappa_z \lambda_i^2 - \kappa_x \alpha_m^2 - \beta_n^2$, ϕ_n

289 and X_n equal $\phi_{m,n}$ and $X_{m,n}$ with $\alpha_m = 0$, respectively, and the eigenvalues λ_0 and λ_i are,

290 respectively, the roots of the following equations:

$$291 \quad e^{2\lambda_0} = \frac{-\gamma \kappa_z \lambda_0^2 + \kappa_z \lambda_0 + \gamma (\kappa_x \alpha_m^2 + \beta_n^2)}{\gamma \kappa_z \lambda_0^2 + \kappa_z \lambda_0 - \gamma (\kappa_x \alpha_m^2 + \beta_n^2)} \quad (40)$$

$$292 \quad \tan \lambda_i = \frac{-\gamma (\kappa_z \lambda_i^2 + \kappa_x \alpha_m^2 + \beta_n^2)}{\kappa_z \lambda_i} \quad (41)$$

293 The determination for those eigenvalues is introduced in the next section. Notice that the

294 solution consists of simple series expanded in β_n , double series expanded in β_n and λ_i (or

295 α_m and β_n), and triple series expanded in α_m , β_n and λ_i .

296 **2.3 Evaluations for β_n , λ_0 and λ_i**

297 Application of Newton's method with proper initial guesses to determine the eigenvalues

298 β_n , λ_0 and λ_i has been proposed by Huang et al. (2014) and is briefly introduced herein. The

299 eigenvalues are situated at the intersection points of the left-hand side (LHS) and RHS

300 functions of Eq. (19) for β_n , Eq. (40) for λ_0 , and Eq. (41) for λ_i . Hence, the initial guesses
 301 for β_n are considered as $\beta_v - \delta$ if $\beta_v > (\kappa_1 \kappa_2)^{0.5}$ and as $\beta_v + \delta$ if $\beta_v < (\kappa_1 \kappa_2)^{0.5}$
 302 where $\beta_v = (2n - 1)\pi/(2 \bar{w}_y)$ and δ is a chosen small value such as 10^{-8} for avoiding being
 303 right at the vertical asymptote. In addition, the guess for λ_0 can be formulated as

$$304 \lambda_{0 \text{ initial}} = \delta + \left\{ -\kappa_z - \sqrt{\kappa_z [\kappa_z + 4 \gamma^2 (\kappa_x \alpha_m^2 + \beta_n^2)]} \right\} / (2\gamma\kappa_z) \quad (42)$$

305 where the RHS second term represents the location of the vertical asymptote derived by letting
 306 the denominator of the RHS function in Eq. (40) to be zero and solving λ_0 in the resultant
 307 equation. Moreover, the guessed value for λ_i is $(2i - 1)\pi/2 + \delta$.

308 **2.4 Head solution for radial collector well**

309 The lateral of RCW is approximately represented by a line sink composed of a series of
 310 adjoining point sinks. The locations of these point sinks are expressed in terms of $(\bar{x}_0 + \bar{l} \cos \theta,$
 311 $\bar{y}_0 + \bar{l} \sin \theta, \bar{z}_0)$ where $(\bar{x}_0, \bar{y}_0, \bar{z}_0) = (x_0/y_0, 1, z_0/H)$ is the central of the lateral, and \bar{l} is
 312 a variable to define different locations of the point sink. The solution of head $\bar{h}_w(\bar{x}, \bar{y}, \bar{z}, \bar{t})$ for
 313 a lateral can therefore be derived by substituting $\bar{x}'_0 = \bar{x}_0 + \bar{l} \cos \theta$, $\bar{y}'_0 = 1 + \bar{l} \sin \theta$ and
 314 $\bar{z}'_0 = \bar{z}_0$ into the point-sink solution, Eq. (30), then by integrating the resultant solution to \bar{l} ,
 315 and finally by dividing the integration result into the sum of lateral lengths. The derivation can
 316 be denoted as

$$317 \bar{h}_w(\bar{x}, \bar{y}, \bar{z}, \bar{t}) = (\sum_{k=1}^N \bar{L}_k)^{-1} \sum_{k=1}^N \int_0^{\bar{L}_k} \bar{h}(\bar{x}, \bar{y}, \bar{z}, \bar{t}) d\bar{l} \quad (43)$$

318 where $\bar{L}_k = L_k/y_0$ is the k -th dimensionless lateral length. Note that the integration variable
 319 \bar{l} (i.e., \bar{x}'_0 and \bar{y}'_0) appears only in X_n and $X_{m,n}$ in Eq. (31). The integral in Eq. (43) can
 320 thus be done analytically by integrating X_n and $X_{m,n}$ with respect to \bar{l} . After the integration,
 321 Eq. (43) can be expressed as

$$322 \bar{h}_w(\bar{x}, \bar{y}, \bar{z}, \bar{t}) = (\sum_{k=1}^N \bar{L}_k)^{-1} \sum_{k=1}^N \begin{cases} \Phi(-\bar{z}_0, \bar{z}, 1) & \text{for } -\bar{z}_0 \leq \bar{z} \leq 0 \\ \Phi(\bar{z}, \bar{z}_0, -1) & \text{for } -1 \leq \bar{z} \leq -\bar{z}_0 \end{cases} \quad (44)$$

323 where Φ is defined by Eqs. (31) – (38), and X_n and $X_{m,n}$ in Eq. (31) are replaced,

324 respectively, by

$$325 \quad X_{n,k} = -G_k / (\beta_n \sin \theta_k) \quad (45)$$

326 and

$$327 \quad X_{m,n,k} = \frac{\alpha_m F_k \cos \theta_k + \beta_n G_k \sin \theta_k}{\alpha_m^2 \cos^2 \theta_k - \beta_n^2 \sin^2 \theta_k} \quad (46)$$

328 with

$$329 \quad F_k = \sin(X\alpha_m) [\beta_n \cos(Y\beta_n) + \kappa_1 \sin(Y\beta_n)] - \sin(\bar{x}_0 \alpha_m) (\beta_n \cos \beta_n + \kappa_1 \sin \beta_n) \quad (47)$$

$$330 \quad G_k = \cos(X\alpha_m) [\kappa_1 \cos(Y\beta_n) - \beta_n \sin(Y\beta_n)] - \cos(\bar{x}_0 \alpha_m) (\kappa_1 \cos \beta_n - \beta_n \sin \beta_n) \quad (48)$$

331 where $X = \bar{x}_0 + \bar{L}_k \cos \theta_k$ and $Y = 1 + \bar{L}_k \sin \theta_k$. Notice that Eq. (45) is obtained by
 332 substituting $\alpha_m = 0$ into Eq. (46). When $\theta_k = 0$ or π , Eq. (45) reduces to Eq. (49) by
 333 applying L'Hospital's rule.

$$334 \quad X_{n,k} = \bar{L}_k (\beta_n \cos \beta_n + \kappa_1 \sin \beta_n) \quad (49)$$

335 **2.5 SDR solution for radial collector well**

336 On the basis of Darcy's law and the head solution for a RCW, the SDR from streams 1
 337 and 2 can be defined, respectively, as

$$338 \quad SDR_1(\bar{t}) = - \int_{\bar{x}=0}^{\bar{x}=\bar{w}_x} \left(\int_{\bar{z}=-\bar{z}_0}^{\bar{z}=0} \frac{\partial \bar{h}_w}{\partial \bar{y}} d\bar{z} + \int_{\bar{z}=-1}^{\bar{z}=-\bar{z}_0} \frac{\partial \bar{h}_w}{\partial \bar{y}} d\bar{z} \right) d\bar{x} \quad \bar{y} = 0 \quad (50)$$

339 and

$$340 \quad SDR_2(\bar{t}) = \int_{\bar{x}=0}^{\bar{x}=\bar{w}_x} \left(\int_{\bar{z}=-\bar{z}_0}^{\bar{z}=0} \frac{\partial \bar{h}_w}{\partial \bar{y}} d\bar{z} + \int_{\bar{z}=-1}^{\bar{z}=-\bar{z}_0} \frac{\partial \bar{h}_w}{\partial \bar{y}} d\bar{z} \right) d\bar{x} \quad \bar{y} = \bar{w}_y \quad (51)$$

341 Again, the double integrals in both equations can be done analytically. Notice that the series
 342 term of $2 \sum_{m=1}^{\infty} \phi_{m,n} X_{m,n} \cos(\alpha_m \bar{x})$ in Eq. (31) disappears due to the consideration of Eqs.
 343 (3) and (4) and the integration with respect to \bar{x} in Eqs. (50) and (51) when deriving the SDR
 344 solution. The SDR_1 and SDR_2 are therefore expressed in terms of double series and given below:

$$345 \quad SDR_1(\bar{t}) = - \frac{2}{\sum_{k=1}^N \bar{L}_k} \sum_{k=1}^N \sum_{n=1}^{\infty} (\psi'_n + \psi'_{n,0} + \sum_{i=1}^{\infty} \psi'_{n,i}) X_{n,k} Y'_n(0) \quad (52)$$

346 and

$$347 \quad SDR_2(\bar{t}) = \frac{2}{\sum_{k=1}^N \bar{L}_k} \sum_{k=1}^N \sum_{n=1}^{\infty} (\psi'_n + \psi'_{n,0} + \sum_{i=1}^{\infty} \psi'_{n,i}) X_{n,k} Y'_n(\bar{w}_y) \quad (53)$$

348 with

$$349 \quad Y'_n(\bar{y}) = \frac{\kappa_1 \beta_n \cos(\beta_n \bar{y}) - \beta_n^2 \sin(\beta_n \bar{y})}{(\beta_n^2 + \kappa_1^2)[\bar{w}_y + \kappa_2 / (\beta_n^2 + \kappa_2^2)] + \kappa_1} \quad (54)$$

$$350 \quad \psi'_n = -\{\sinh(\bar{z}_0 \lambda'_s) \cosh[(1 - \bar{z}_0) \lambda'_s] + \sinh[(1 - \bar{z}_0) \lambda'_s] \cosh(\bar{z}_0 \lambda'_s)\} / (\kappa_z \lambda_s'^2 \sinh \lambda'_s) \quad (55)$$

$$352 \quad \psi'_{n,0} = -\mu_{n,0}(\theta_{n,0} + \vartheta_{n,0}) / \lambda_0 \quad (56)$$

$$353 \quad \theta_{n,0} = \cosh[(1 - \bar{z}_0) \lambda_0] \{p'_0 \gamma [-1 + \cosh(\bar{z}_0 \lambda_0) + \kappa_z \lambda_0 \sinh(\bar{z}_0 \lambda_0)]\} \quad (57)$$

$$354 \quad \vartheta_{n,0} = \sinh[(1 - \bar{z}_0) \lambda_0] [\kappa_z \lambda_0 \cosh(\bar{z}_0 \lambda_0) + p'_0 \gamma \sinh(\bar{z}_0 \lambda_0)] \quad (58)$$

$$355 \quad \psi'_{n,i} = v_{n,i}(\sigma_{n,i} - \eta_{n,i}) / \lambda_i \quad (59)$$

$$356 \quad \sigma_{n,i} = \cos[(1 - \bar{z}_0) \lambda_i] \{p'_i \gamma [-1 + \cos(\bar{z}_0 \lambda_i)] - \kappa_z \lambda_i \sin(\bar{z}_0 \lambda_i)\} \quad (60)$$

$$357 \quad \eta_{n,i} = \sin[(1 - \bar{z}_0) \lambda_i] [\kappa_z \lambda_i \cos(\bar{z}_0 \lambda_i) + p'_i \gamma \sin(\bar{z}_0 \lambda_i)] \quad (61)$$

358 where $\lambda'_s = \beta_n / \sqrt{\kappa_z}$; $p'_0 = \kappa_z \lambda_0^2 - \beta_n^2$; $p'_i = -\kappa_z \lambda_i^2 - \beta_n^2$; $\mu_{n,0}$ equals $\mu_{m,n,0}$ in Eq. (36)

359 with $\alpha_m = 0$; $v_{n,i}$ equals $v_{m,n,i}$ in Eq. (37) with $\alpha_m = 0$; $X_{n,k}$ is defined in Eq. (45) for

360 $\theta_k \neq 0$ or π and Eq. (49) for $\theta_k = 0$ or π ; and λ_0 and λ_i are the roots of Eqs. (40) and

361 (41) with $\alpha_m = 0$, respectively.

362

363 2.6 Special cases of the present solution

364 2.6.1 Confined aquifer of finite extent

365 If $\gamma = 0$ (i.e., $S_y = 0$ in Eq. (8)), the top boundary is regarded as an impermeable stratum.

366 The aquifer is then a confined system. Under this circumstance, Eq. (40) reduces to $e^{2\lambda_0} = 1$

367 having the root of $\lambda_0 = 0$, and Eq. (41) yields $\tan \lambda_i = 0$ having the roots of $\lambda_i = i\pi$ where

368 $i \in 1, 2, 3, \dots, \infty$. With $\gamma = 0$, $\lambda_0 = 0$ and $\lambda_i = i\pi$, the head solution for a confined aquifer

369 can be expressed as Eq. (44) with Eqs. (31) – (38) and (45) – (49) where $\psi_{m,n,0}$ in Eq. (32)

370 is replaced by

$$371 \quad \psi_{m,n,0} = -\exp(p_0 \bar{t})/p_0 \quad (62)$$

372 Similarly, the SDR solution for a confined aquifer can be written as Eqs. (52) and (53) where
373 the RHS function in Eq. (56) reduces to that in Eq. (62) by applying L'Hospital's rule with $\gamma =$
374 0 and $\lambda_0 = 0$.

375 **2.6.2 Confined aquifer of infinite extent**

376 The head solution introduced in section 2.6.1 is applicable to spatiotemporal head
377 distributions in confined aquifers of infinite extent before the lateral boundary effect comes.
378 Wang and Yeh (2008) indicated that the time can be quantified, in our notation, as $t = R^2 S_s / (16K_y)$
379 (i.e., $\bar{t} = R^2 / (16y_0^2)$ for dimensionless time) where R is the shortest distance between a RCW
380 and aquifer lateral boundary. Prior to the time, the present head solution with $N = 1$ for a
381 horizontal well in a confined aquifer gives very close results given in Zhan et al. (2001).

382 **2.6.3 Unconfined aquifer of infinite extent**

383 Prior to the beginning time mentioned in section 2.6.2, the absolute value calculated by
384 the present head solution, Eqs. (44) with $N = 1$, represents drawdown induced by a horizontal
385 well in unconfined aquifers of infinite extent. The calculated drawdown should be close to that
386 from Zhan and Zlotnik (2002) solution for the case of the instantaneous drainage from water
387 table decline.

388 **2.6.4 Unconfined aquifer of semi-infinite extent**

389 When $\kappa_1 \rightarrow \infty$ (i.e., $b_1 = 0$), Eq. (14) reduces to the Dirichlet condition of $\bar{h} = 0$ for stream
390 1 in the absence from a low-permeability streambed, and Eq. (19) becomes $\tan(\beta_n \bar{w}_y) =$
391 $-\beta_n / \kappa_2$. In addition, the boundary effect occurring at the other three sides of the aquifer can
392 be neglected prior to the beginning time. Moreover, when $N = 1$ and $\theta_1 = 0$, a RCW can be
393 regarded as a horizontal well parallel to stream 1. Under these three conditions, the present
394 head and SDR predictions are close to those in Huang et al. (2011), the head solution of which

395 agrees well with measured data from a field experiment executed by Mohamed and Rushton
 396 (2006). On the other hand, before the time when the boundary effect occurs at $\bar{x} = 0$, $\bar{x} = \bar{w}_x$
 397 and $\bar{y} = \bar{w}_y$, the present head and SDR solutions for a RCW give close predictions to those in
 398 Huang et al. (2012), the head and SDR solutions of which agree well with observation data
 399 taken from two field experiments carried out by Schafer (2006) and Jasperse (2009),
 400 respectively.

401 2.7 Sensitivity analysis

402 The hydraulic parameters determined from field observed data are inevitably subject to
 403 measurement errors. Consequently, head predictions from the analytical model have
 404 uncertainty due to the propagation of measurement errors. Sensitivity analysis can be
 405 considered as a tool of exploring the response of the head to the change in a specific parameter
 406 (Zheng and Bennett, 2002). One may define the normalized sensitivity coefficient as

$$407 \quad S_{i,t} = \frac{P_i}{H} \frac{\partial h}{\partial P_i} \quad (63)$$

408 where $S_{i,t}$ is the normalized sensitivity coefficient for the i th parameter at time t , and P_i
 409 represents the magnitude of the i th parameter. Eq. (63) can be approximated as

$$410 \quad S_{i,t} = \frac{h(P_i + \Delta P_i) - h(P_i)}{\Delta P_i} \times \frac{P_i}{H} \quad (64)$$

411 where ΔP_i is an increment chosen as $10^{-3} P_i$ (Yeh et al., 2008).

412 3. Results and discussion

413 This section demonstrates head and SDR predictions and explores some physical insights
 414 regarding flow behavior. In section 3.1, equipotential lines are drawn to identify 3-D or 2-D
 415 flow without the vertical flow at a specific region. In section 3.2, the influence of anisotropy
 416 on spatial head and temporal SDR distributions is studied. In section 3.3, the sensitivity analysis
 417 is performed to investigate the response of the head to the change in each hydraulic parameter.
 418 In section 3.4, the effects of the vertical flow and well depth on temporal SDR distributions for

419 confined and unconfined aquifers are investigated. For conciseness, we consider a RCW with
 420 two laterals with $N = 2$, $\bar{L}_1 = \bar{L}_2 = 0.5$, $\theta_1 = 0$ and $\theta_2 = \pi$. The well can be viewed as a
 421 horizontal well parallel to streams 1 and 2. The default values for the other dimensionless
 422 parameters are $\bar{w}_x = \bar{w}_y = 2$, $\gamma = 100$, $\bar{x}_0 = 1$, $\bar{y}_0 = 1$, $\bar{z}_0 = 0.5$, $\kappa_x = \kappa_z = 1$, and $\kappa_1 = \kappa_2 =$
 423 20.

424 3.1 Identification of 3-D or 2-D flow at observation point

425 Most existing models assume 2-D flow with neglecting the vertical flow for pumping at a
 426 horizontal well (e.g., Mohamed and Rushton, 2006; Haitjema et al., 2010). The head
 427 distributions predicted by those models are inaccurate if an observation point is close to the
 428 region where the vertical flow prevails. Figure 2 demonstrates the equipotential lines predicted
 429 by the present solution for a horizontal well in an unconfined aquifer for $\bar{x}_0 = 10$, $\bar{w}_x = \bar{w}_y =$
 430 20 and $\kappa_z = 0.1, 1$, and 10. The well is located at $9.5 \leq \bar{x} \leq 10.5$, $\bar{y} = 1$ and $\bar{z} = 0.5$ as
 431 illustrated in the figure. The equipotential lines are based on steady-state head distributions
 432 plotted by Eq. (44) with $\bar{y} = 1$ and $\bar{t} = 10^7$. When $\kappa_z = 0.1$, in the range of $10 \leq \bar{x} \leq 13.66$,
 433 the contours of the hydraulic head are in a curved path, and the flow toward the well is thus
 434 slanted. Moreover, the range decreases to $10 \leq \bar{x} \leq 11.5$ when $\kappa_z = 1$ and to $10 \leq \bar{x} \leq 10.82$
 435 when $\kappa_z = 10$. Beyond these ranges, the head contours are nearly vertical, and the flow is
 436 essentially horizontal. Define $\bar{d} = d/y_0$ as a shortest dimensionless horizontal distance between
 437 the well and a nearest location of only horizontal flow. The \bar{d} is therefore chosen as 3.16, 1
 438 and 0.32 for the cases of $\kappa_z = 0.1, 1$ and 10, respectively. Substituting $(\kappa_z, \bar{d}) = (0.1, 3.16), (1,$
 439 1) and $(10, 0.32)$ into $\kappa_z \bar{d}^2$ leads to about unity. We may therefore conclude that the vertical
 440 flow at an observation point is negligible if its location is beyond the range of $\bar{d} < \sqrt{1/\kappa_z}$
 441 (i.e., $d < H\sqrt{K_y/K_z}$) for thin aquifers, an observation point far from the well, and/or a small
 442 ratio of K_y/K_z .

443 3.2 Anisotropy analysis of hydraulic head and stream depletion rate

444 Previous articles have seldom analyzed flow behavior for anisotropic aquifers, i.e., κ_x
445 $(K_x/K_y) \neq 1$. Head predictions based on the models, developed for isotropic aquifers, will be
446 inaccurate if $\kappa_x \neq 1$. Consider $\bar{w}_x = \bar{w}_y = 2$, $\bar{t} = 10^7$ for steady-state head distributions, and
447 a RCW with $\bar{L}_1 = \bar{L}_2 = 0.25$, $\theta_1 = 0$, $\theta_2 = \pi$, and $(\bar{x}_0, \bar{y}_0, \bar{z}_0) = (1, 1, -0.5)$ for symmetry. The
448 contours of the dimensionless head at $\bar{z} = -0.5$ are shown in Figures 3(a) – 3(d) for $\kappa_x = 1$,
449 10 and 50, 10^{-3} , and 10^{-4} , respectively. The figure indicates that the anisotropy causes a
450 significant effect on the head distributions in comparison with the case of $\kappa_x = 1$. In Figure 3(b),
451 the contours exhibit smooth curves in the strip regions of $1 \leq \bar{y} \leq 1.45$ for the case of $\kappa_x = 10$
452 and $1 \leq \bar{y} \leq 1.2$ for the case of $\kappa_x = 50$. For the region of $\bar{y} \geq 1.45$, the predicted heads for
453 both cases agree well, and all the contour lines are parallel, indicating that the flow is essentially
454 unidirectional. Substituting $(\kappa_x, \bar{y}) = (10, 1.45)$ and $(50, 1.2)$ into $\kappa_x (\bar{y} - 1)^2$ results in a value
455 about 2. Accordingly, we may draw the conclusion that plots from the inequality of
456 $\kappa_x (\bar{y} - 1)^2 \leq 2$ indicate the strip region for κ_x being greater than 10. Some existing models
457 assuming 2-D flow in a vertical plane with neglecting the flow component along a horizontal
458 well give accurate head predictions beyond the region (e.g., Anderson, 2000; Anderson, 2003;
459 Kompani-Zare et al., 2005).

460 Aquifers with $K_y H \geq 10^3$ m²/day can efficiently produce plenty of water from a well.
461 RCWs usually operate with $Q \leq 10^5$ m³/day for field experiments (e.g., Schafer, 2006; Jasperse,
462 2009). We therefore define significant dimensionless head drop as $|\bar{h}| > 10^{-5}$ (i.e., $|h| > 1$
463 mm). The anisotropy of $\kappa_x < 1$ produces the drop in the strip areas of $1 \leq \bar{x} \leq 1.48$ for the case
464 of $\kappa_x = 10^{-3}$ in Figure 3(c) and $1 \leq \bar{x} \leq 1.32$ for the case of $\kappa_x = 10^{-4}$ in Figure 3(d). Substituting
465 $(\kappa_x, \bar{x}) = (10^{-3}, 1.48)$ and $(10^{-4}, 1.32)$ into $(\bar{x} - \bar{x}_0 - \bar{L}_1)^2 / \kappa_x$ approximates 52.9. This result
466 leads to the conclusion that the area can be determined by the inequalities of $(\bar{x} - \bar{x}_0 - \bar{L}_1)^2 \leq$

467 $52.9\kappa_x$ and $(\bar{x} - \bar{x}_0 + \bar{L}_2)^2 \leq 52.9\kappa_x$ for any value of κ_x in the range $\kappa_x < 1$. For a RCW with
468 irregular lateral configurations, the inequalities become $(\bar{x} - \max \bar{x}_k)^2 \leq 52.9 \kappa_x$ and
469 $(\bar{x} - \min \bar{x}_k)^2 \leq 52.9 \kappa_x$ where \bar{x}_k is coordinate \bar{x} of the far end of the k -th lateral. The
470 conclusion applies in principle to reduction in grid points for numerical solutions based on
471 finite difference methods or finite element methods. On the other hand, we have found that Eq.
472 (52) or (53) with various κ_x predicts the same temporal SDR distribution (not shown),
473 indicating that the SDR is independent of κ_x .

474 3.3 Sensitivity analysis of hydraulic head

475 Consider an unconfined aquifer of $H = 20$ m and $w_x = w_y = 800$ m with a RCW having
476 two laterals of $L_1 = L_2 = 50$ m, $\theta_1 = 0$ and $\theta_2 = \pi$ and two piezometers installed at point A of
477 (400 m, 340 m, -10 m) and point B of (400 m, 80 m, -10 m) illustrated in Figure 4. As
478 discussed in section 3.1, the temporal head distribution at point A exhibits the unconfined
479 behavior in Figure 4(a) because of $\kappa_z \bar{d}^2 < 1$ while at point B displays the confined one in Figure
480 4(b) due to $\kappa_z \bar{d}^2 > 1$. The sensitivity analysis is conducted with the aid of equation (64) to
481 observe head responses at these two piezometers to the change in each of K_x , K_y , K_z , S_s , S_y , K_1 ,
482 L_1 and z_0 . The temporal distribution curves of the normalized sensitivity coefficients for those
483 eight parameters are shown in Figures 4(a) for point A and 4(b) for point B when $K_x = K_y = 1$
484 m/day, $K_z = 0.1$ m/day, $S_s = 10^{-5}$ m⁻¹, $S_y = 0.2$, $K_1 = K_2 = 0.1$ m/day, $b_1 = b_2 = 1$ m, $Q = 100$
485 m³/day, $x_0 = y_0 = 400$ m, and $z_0 = 10$ m. The figure demonstrates that the hydraulic heads at
486 both piezometers are most sensitive to the change in K_y , second sensitive to the change in K_x
487 and thirdly sensitive to the change in S_y , indicating that K_y , K_x and S_y are the most crucial factors
488 in designing a pumping system. This figure also shows that the heads at point A is sensitive to
489 the change in S_s at the early period of 4×10^{-3} day $< t < 10^{-1}$ day but at point B is insensitive to
490 the change over the entire period. In addition, the head at point A is sensitive to the changes in
491 K_z and z_0 due to 3-D flow (i.e., $\kappa_z \bar{d}^2 < 1$) as discussed in section 3.1. In contrast, the head at

492 point B is insensitive to the changes in K_z and z_0 because the vertical flow diminishes (i.e.,
493 $\kappa_z \bar{a}^2 > 1$). Moreover, the head at point A is sensitive to the change in L_1 but the head at point
494 B is not because its location is far away from the well. Furthermore, the normalized sensitivity
495 coefficient of K_1 for point A away from stream 1 approaches zero but for point B in the vicinity
496 of stream 1 increases with time and finally maintains a certain value at the steady state.
497 Regarding the sensitivity analysis of SDR, Huang et al. (2014) has performed the sensitivity
498 analysis of normalized coefficients of SDR_1 to the changes in K_y , K_1 and S_s for a confined
499 aquifer and in K_y , K_z , K_1 , S_s and S_y for an unconfined aquifer.

500 **3.4 Effects of vertical flow and well depth on stream depletion rate**

501 Huang et al. (2014) reveals that the effect of the vertical flow on SDR induced by a vertical
502 well is dominated by the magnitude of the key factor κ_z (i.e., $K_z y_0^2 / (K_y H^2)$) where y_0 herein
503 is a distance between stream 1 and the vertical well. They concluded that the effect is negligible
504 when $\kappa_z \geq 10$ for a leaky aquifer. The factor should be replaced by $\kappa_z \bar{a}^2$ (i.e., $K_z a^2 / (K_y H^2)$)
505 where a is a shortest distance measured from stream 1 to the end of a lateral of a RCW, and
506 $\bar{a} = a / y_0 = 1$ in this study due to $N = 2$, $\theta_1 = 0$ and $\theta_2 = \pi$. We investigate SDR in response to
507 various \bar{z}_0 and $\kappa_z \bar{a}$ for unconfined and confined aquifers. The temporal SDR_1 distributions
508 predicted by Eq. (52) for stream 1 adjacent to an unconfined aquifer are shown in Fig. 5(a) for
509 $\bar{z}_0 = 0.5$ and $\kappa_z \bar{a}^2 = 0.01, 0.1, 1, 10, 20$ and 30 and Fig. 5(b) for $\kappa_z \bar{a}^2 = 1$ and 30 when $\bar{z}_0 =$
510 $0.1, 0.3, 0.5, 0.7$ and 0.9 . The curves of SDR_1 versus \bar{t} is plotted in both panels by the present
511 SDR solution for a confined aquifer. In Fig. 5(a), the present solution for an unconfined aquifer
512 predicts a close SDR_1 to that for the confined aquifer when $\kappa_z \bar{a}^2 = 0.01$, indicating that the
513 vertical flow in the unconfined aquifer is ignorable. The SDR_1 for the unconfined aquifer with
514 $\kappa_z \bar{a}^2 = 30$ behaves like that for a confined one, indicating the vertical flow is also ignorable.
515 The SDR_1 is therefore independent of well depths \bar{z}_0 when $\kappa_z \bar{a}^2 = 30$ as shown in Fig. 5(b).
516 We may therefore conclude that, under the condition of $\kappa_z \bar{a}^2 \leq 0.01$ or $\kappa_z \bar{a}^2 \geq 30$, a 2-D

517 horizontal flow model can give good predictions in SDR_1 for unconfined aquifers. In contrast,
518 SDR_1 increases with decreasing $\kappa_z \bar{a}^2$ when $0.01 < \kappa_z \bar{a}^2 < 30$ in Fig. 5(a), indicating that the
519 vertical flow component induced by pumping in unconfined aquifers significantly affects SDR_1 .
520 The effect of well depth \bar{z}_0 on SDR_1 is also significant as shown in Fig. 5(b) when $\kappa_z \bar{a}^2 = 1$.
521 Obviously, the vertical flow effect should be considered in a model when $0.01 < \kappa_z \bar{a}^2 < 30$
522 for unconfined aquifers.

523 It is interesting to note that the SDR_1 or SDR_2 induced by two laterals (i.e., $\theta_1 = 0$ and θ_2
524 $= \pi$) parallel to the streams adjacent to a confined aquifer is independent of $\kappa_z \bar{a}^2$ and \bar{z}_0 but
525 depends on aquifer width of \bar{w}_y . The temporal SDR distribution curves based on Eqs. (52) and
526 (53) with $\gamma = 0$ for a confined aquifer with $\bar{w}_y = 2, 4, 6, 10$ and 20 are plotted in Fig. 6. The
527 dimensionless distance between the well and stream 1 is set to unity (i.e., $\bar{y}_0 = 1$) for each
528 case. The SDR_1 predicted by Hunt (1999) solution based on a vertical well in a confined aquifer
529 extending infinitely is considered. The present solution for each \bar{w}_y gives the same SDR_1 as
530 the Hunt solution before the time when stream 2 contributes filtration water to the aquifer and
531 influences the supply of SDR_1 . It is interesting to note that the sum of steady-state SDR_1 and
532 SDR_2 is always unity for a fixed \bar{w}_y . The former and latter can be estimated by $(\bar{w}_y - 1)/\bar{w}_y$
533 and $1/\bar{w}_y$, respectively. Such a result corresponds with that in Sun and Zhan (2007) which
534 investigates the distribution of steady-state SDR_1 and SDR_2 induced by a vertical well.

535 **4. Concluding remarks**

536 This study develops a new analytical model describing 3-D flow induced by a RCW in a
537 rectangular confined or unconfined aquifer bounded by two parallel streams and no-flow
538 stratum in the other two sides. The flow equation in terms of the hydraulic head with a point
539 sink term is employed. Both streams fully penetrate the aquifer and are under the Robin
540 condition in the presence of low-permeability streambeds. A first-order free surface equation

541 (8) describing the water table decline gives good predictions when the conditions $|h|/H \leq 0.1$
542 and $|\partial h/\partial x| + |\partial h/\partial y| \leq 0.01$ are satisfied. The flux across the well screen might be
543 uniform on a lateral within 150 m. The head solution for the point sink is expressed in terms of
544 a triple series derived by the methods of Laplace transform and finite integral transform. The
545 head solution for a RCW is then obtained by integrating the point-sink solution along the
546 laterals and dividing the integration result by the sum of lateral lengths. The integration can be
547 done analytically due to the aquifer of finite extent with Eqs. (3) – (6). On the basis of Darcy’s
548 law and the head solution, the SDR solution for two streams can also be acquired. The double
549 integrals of defining the SDR in Eqs. (50) and (51) can also be done analytically due to
550 considerations of Eqs. (3) – (6). The sensitivity analysis is performed to explore the response
551 of the head to the change in each of the hydraulic parameters and variables. New findings
552 regarding the responses of flow and SDR to pumping at a RCW are summarized below:

- 553 1. Groundwater flow in a region based on $\bar{d} < \sqrt{1/\kappa_z}$ is 3-D, and temporal head
554 distributions exhibit the unconfined behavior. A mathematical model should consider 3-D
555 flow when predicting the hydraulic head in the region. Beyond this region, groundwater
556 flow is horizontal, and temporal head distributions display the confined behavior. A 2-D
557 flow model can predict accurate hydraulic head.
- 558 2. The aquifer anisotropy of $\kappa_x > 10$ causes unidirectional flow in the strip region determined
559 based on $\kappa_x (\bar{y} - 1)^2 > 2$ for a horizontal well. Existing models assuming 2-D flow in a
560 vertical plane with neglecting the flow component along the well give accurate head
561 predictions in the region.
- 562 3. The aquifer anisotropy of $\kappa_x < 1$ produces significant change in the head (i.e., $|\bar{h}| > 10^{-5}$
563 or $|h| > 1$ mm) in the strip area determined by $(\bar{x} - \max \bar{x}_k)^2 \leq 52.9 \kappa_x$ and $(\bar{x} -$
564 $\min \bar{x}_k)^2 \leq 52.9 \kappa_x$ for a RCW with irregular lateral configurations.
- 565 4. The hydraulic head in the whole domain is most sensitive to the change in K_y , second

566 sensitive to the change in K_x , and thirdly sensitive to the change in S_y . They are thus the
567 most crucial factors in designing a pumping system.

568 5. The hydraulic head is sensitive to changes in K_z , S_s , z_0 and L_k in the region of $\bar{d} <$
569 $\sqrt{1/\kappa_z}$ and is insensitive to the changes of them beyond the region.

570 6. The hydraulic head at observation points near stream 1 is sensitive to the change in K_1 but
571 away from the stream isn't.

572 7. The effect of the vertical flow on SDR is ignorable when $\kappa_z \bar{a}^2 \leq 0.01$ or $\kappa_z \bar{a}^2 \geq 30$ for
573 unconfined aquifers. In contrast, neglecting the effect will underestimate SDR when 0.01
574 $< \kappa_z \bar{a}^2 < 30$.

575 8. For unconfined aquifers, SDR increases with dimensionless well depth \bar{z}_0 when $0.01 < \kappa_z$
576 < 30 and is independent of \bar{z}_0 when $\kappa_z \leq 0.01$ or $\kappa_z \geq 30$. For confined aquifers, SDR is
577 independent of \bar{z}_0 and κ_z . For both kinds of aquifers, the distribution curve of SDR versus
578 \bar{t} is independent of aquifer anisotropy κ_x .

579

580 **Acknowledgements.**

581 Research leading to this paper has been partially supported by the grants from the Taiwan
582 Ministry of Science and Technology under the contract NSC 102 – 2221 – E – 009 – 072 –
583 MY2, MOST 103 – 2221 – E – 009 – 156, and MOST 104 – 2221 – E – 009 – 148 – MY2.

584

585 **Appendix A: Finite integral transform**

586 Latinopoulos (1985) provided the finite integral transform for a rectangular aquifer
587 domain where each side can be under either the Dirichlet, no-flow, or Robin condition. The
588 transform associated with the boundary conditions, Eqs. (12) – (15), is defined as

$$589 \tilde{h}(\alpha_m, \beta_n) = \mathfrak{S}\{\bar{h}(\bar{x}, \bar{y})\} = \int_0^{\bar{w}_x} \int_0^{\bar{w}_y} \bar{h}(\bar{x}, \bar{y}) \cos(\alpha_m \bar{x}) K(\bar{y}) d\bar{y} d\bar{x} \quad (\text{A1})$$

590 with

591
$$K(\bar{y}) = \sqrt{2} \frac{\beta_n \cos(\beta_n \bar{y}) + \kappa_1 \sin(\beta_n \bar{y})}{\sqrt{(\beta_n^2 + \kappa_1^2)[\bar{w}_y + \kappa_2 / (\beta_n^2 + \kappa_2^2)] + \kappa_1}} \quad (\text{A2})$$

592 where $\cos(\alpha_m \bar{x}) K(\bar{y})$ is the kernel function. According to Latinopoulos (1985, Eq. (9)), the
 593 transform has the property of

594
$$\Im \left\{ \kappa_x \frac{\partial^2 \bar{h}}{\partial \bar{x}^2} + \frac{\partial^2 \bar{h}}{\partial \bar{y}^2} \right\} = -(\kappa_x \alpha_m^2 + \beta_n^2) \tilde{h}(\alpha_m, \beta_n) \quad (\text{A3})$$

595 The formula for the inverse finite integral transform can be written as (Latinopoulos, 1985, Eq.
 596 (14))

597
$$\bar{h}(\bar{x}, \bar{y}) = \Im^{-1} \left\{ \tilde{h}(\alpha_m, \beta_n) \right\} = \frac{1}{\bar{w}_x} \left[\sum_{n=1}^{\infty} \tilde{h}(0, \beta_n) K(\bar{y}) + 2 \sum_{m=1}^{\infty} \sum_{n=1}^{\infty} \tilde{h}(\alpha_m, \beta_n) \cos(\alpha_m \bar{x}) K(\bar{y}) \right] \quad (\text{A4})$$

598

599 **Appendix B: Derivation of equation (31)**

600 The function of p in Eq. (28) is defined as

601
$$F(p) = \frac{\cosh[(1+a)\lambda] [-\kappa_z \lambda \cosh(b\lambda) + c p \gamma \sinh(b\lambda)]}{p \kappa_z \lambda (p \gamma \cosh \lambda + \kappa_z \lambda \sinh \lambda)} \quad (\text{B1})$$

602 Notice that the term $\cos(\alpha_m \bar{x}_0) K(\bar{y}_0)$ in Eq. (28) is excluded because it is independent of p .
 603 $F(p)$ is a single-value function with respect to p . On the basis of the residue theorem, the
 604 inverse Laplace transform for $F(p)$ equals the summation of residues of poles in the complex
 605 plane. The residue of a simple pole can be derived according to the formula below:

606
$$\text{Res}|_{p=p_i} = \lim_{p \rightarrow p_i} F(p) \exp(p\bar{t}) (p - p_i) \quad (\text{B2})$$

607 where p_i is the location of the pole in the complex plane.

608 The locations of poles are the roots of the equation obtained by letting the denominator in
 609 Eq. (B1) to be zero, denoted as

610
$$p \kappa_z \lambda (p \gamma \cosh \lambda + \kappa_z \lambda \sinh \lambda) = 0 \quad (\text{B3})$$

611 where λ is defined in Eq. (29). Notice that $p = -\kappa_x \alpha_m^2 - \beta_n^2$ obtained by $\lambda = 0$ is not a
 612 pole in spite of being a root. Apparently, one pole is at $p = 0$, and the residue based on Eq. (B2)

613 with $p_i = 0$ is expressed as

$$614 \text{ Res}|_{p=0} = \lim_{p \rightarrow 0} \frac{\cosh[(1+a)\lambda][-\kappa_z \lambda \cosh(b\lambda) + cp\gamma \sinh(b\lambda)]}{\kappa_z \lambda (p\gamma \cosh \lambda + \kappa_z \lambda \sinh \lambda)} \exp(p\bar{t}) \quad (\text{B4})$$

615 Eq. (B4) with $p = 0$ and $\lambda = \lambda_s$ reduces to $\psi_{m,n}$ in Eq. (33).

616 Other poles are determined by the equation of

$$617 p \gamma \cosh \lambda + \kappa_z \lambda \sinh \lambda = 0 \quad (\text{B5})$$

618 which comes from Eq. (B3). One pole is at $p = p_0$ between $p = 0$ and $p = -\kappa_x \alpha_m^2 - \beta_n^2$ in

619 the negative part of the real axis. Newton's method can be used to obtain the value of p_0 . In

620 order to have proper initial guess for Newton's method, we let $\lambda = \lambda_0$ and then have $p =$

621 $\kappa_z \lambda_0^2 - \kappa_x \alpha_m^2 - \beta_n^2$ based on Eq. (29). Substituting $\lambda = \lambda_0$, $p = \kappa_z \lambda_0^2 - \kappa_x \alpha_m^2 - \beta_n^2$,

622 $\cosh \lambda_0 = (e^{\lambda_0} + e^{-\lambda_0})/2$ and $\sinh \lambda_0 = (e^{\lambda_0} - e^{-\lambda_0})/2$ into Eq. (B5) and rearranging the

623 result leads to Eq. (40). Initial guess for finding root λ_0 of Eq. (40) is discussed in section 2.3.

624 With known value of λ_0 , one can obtain $p_0 = \kappa_z \lambda_0^2 - \kappa_x \alpha_m^2 - \beta_n^2$. According to Eq. (B2),

625 the residue of the simple pole at $p = p_0$ is written as

$$626 \text{ Res}|_{p=p_0} = \lim_{p \rightarrow p_0} \frac{\cosh[(1+a)\lambda][-\kappa_z \lambda \cosh(b\lambda) + cp\gamma \sinh(b\lambda)]}{p \kappa_z \lambda (p\gamma \cosh \lambda + \kappa_z \lambda \sinh \lambda)} \exp(p\bar{t}) (p - p_0) \quad (\text{B6})$$

627 where both the denominator and nominator equal zero when $p = p_0$. Applying L'Hospital's

628 Rule to Eq. (B6) results in

$$629 \text{ Res}|_{p=p_0} = \lim_{p \rightarrow p_0} \frac{2 \cosh[(1+a)\lambda][-\kappa_z \lambda \cosh(b\lambda) + cp\gamma \sinh(b\lambda)]}{p[(1+2\gamma)\kappa_z \lambda \cosh \lambda + (\gamma p + \kappa_z) \sinh \lambda]} \exp(p\bar{t}) \quad (\text{B7})$$

630 Eq. (B7) with $p = p_0$ and $\lambda = \lambda_0$ reduces to $\psi_{m,n,0}$ in Eq. (34).

631 On the other hand, infinite poles are at $p = p_i$ behind $p = -\kappa_x \alpha_m^2 - \beta_n^2$. Similar to the

632 derivation of Eq. (40), we let $\lambda = \sqrt{-1}\lambda_i$ and then have $p = -\kappa_z \lambda_i^2 - \kappa_x \alpha_m^2 - \beta_n^2$ based

633 on Eq. (29). Substituting $\lambda = \sqrt{-1}\lambda_i$, $p = -\kappa_z \lambda_i^2 - \kappa_x \alpha_m^2 - \beta_n^2$, $\cosh \lambda = \cos \lambda_i$ and

634 $\sinh \lambda = \sqrt{-1} \sin \lambda_i$ into Eq. (B3) and rearranging the result yields Eq. (41). The

635 determination of λ_i is discussed in section 2.3. With known value λ_i , one can have $p_i =$

636 $-\kappa_z \lambda_i^2 - \kappa_x \alpha_m^2 - \beta_n^2$. The residues of those simple poles at $p=p_i$ can be expressed as $\psi_{m,n,i}$
637 in Eq. (35) by substituting $p_0 = p_i$, $p = p_i$, $\lambda = \sqrt{-1}\lambda_i$, $\cosh \lambda = \cos \lambda_i$ and $\sinh \lambda =$
638 $\sqrt{-1} \sin \lambda_i$ into Eq. (B7). Eventually, the inverse Laplace transform for $F(p)$ equals the sum
639 of those residues (i.e., $\phi_{m,n} = \psi_{m,n} + \psi_{m,n,0} + \sum_{i=1}^{\infty} \psi_{m,n,i}$). The time-domain result of
640 $\Omega(a, b, c)$ in Eq. (28) is then obtained as $\phi_{m,n} \cos(\alpha_m \bar{x}_0) K(\bar{y}_0)$. By substituting
641 $\tilde{h}(\alpha_m, \beta_n) = \phi_{m,n} \cos(\alpha_m \bar{x}_0) K(\bar{y}_0)$ and $\tilde{h}(0, \beta_n) = \phi_n K(\bar{y}_0)$ into Eq. (A4) and letting
642 $\bar{h}(\bar{x}, \bar{y})$ to be $\Phi(a, b, c)$, the inverse finite integral transform for the result can be derived as

$$643 \quad \Phi(a, b, c) = \frac{1}{w_x} \left[\sum_{n=1}^{\infty} (\phi_n K(\bar{y}_0) K(\bar{y}) + \right. \\
644 \quad \left. 2 \sum_{m=1}^{\infty} \phi_{m,n} \cos(\alpha_m \bar{x}_0) K(\bar{y}_0) \cos(\alpha_m \bar{x}) K(\bar{y})) \right] \quad (\text{B8})$$

645 Moreover, Eq. (B8) reduces to Eq. (31) when letting the terms of $K(\bar{y}_0) K(\bar{y})$ and
646 $\cos(\alpha_m \bar{x}_0) K(\bar{y}_0) K(\bar{y})$ to be $2X_n Y_n$ and $2X_{m,n} Y_n$, respectively.

647

648 References

649 Anderson, E. I.: The method of images for leaky boundaries, *Adv. Water Resour.*, 23, 461–474,
650 doi:10.1016/S0309-1708(99)00044-5, 2000.

651 Anderson, E. I.: An analytical solution representing groundwater-surface water interaction,
652 *Water Resour. Res.*, 39(3), 1071, doi:10.1029/2002WR001536, 2003.

653 Anderson, E. I.: Stable pumping rates for horizontal wells in bank filtration systems, *Adv.*
654 *Water Resour.*, 54, 57–66, doi:10.1016/j.advwatres.2012.12.012, 2013.

655 Bear, J.: *Hydraulics of Groundwater*, McGraw-Hill, New York, 84, 1979.

656 Charbeneau, R. J.: *Groundwater Hydraulics and Pollutant Transport*, Prentice-Hall, NJ, 57,
657 2000.

658 Chen, C. X., Wan, J. W., and Zhan, H. B.: Theoretical and experimental studies of coupled
659 seepage-pipe flow to a horizontal well, *J. Hydrol.*, 281(1–2), 159–171,

660 doi:10.1016/S0022-1694(03)00207-5, 2003.

661 Chen, X., Dong, W., Ou, G., Wang, Z., and Liu, C.: Gaining and losing stream reaches have
662 opposite hydraulic conductivity distribution patterns, *Hydrol. Earth Syst. Sci.*, 17, 2569–
663 2579, doi:10.5194/hess-17-2569-2013, 2013.

664 Exner-Kittridge, M., Salinas, J. L., and Zessner, M.: An evaluation of analytical stream to
665 groundwater exchange models: a comparison of gross exchanges based on different spatial
666 flow distribution assumptions, *Hydrol. Earth Syst. Sci.*, 18, 2715–2734, doi:10.5194/hess-
667 18-2715-2014, 2014.

668 Flipo, N., Mouhri, A., Labarthe, B., Biancamaria, S., Rivière, A., and Weill, P.: Continental
669 hydrosystem modelling: the concept of nested stream–aquifer interfaces, *Hydrol. Earth
670 Syst. Sci.*, 18, 3121–3149, doi:10.5194/hess-18-3121-2014, 2014.

671 Goldscheider, N., and Drew, D.: *Methods in karst hydrology*, Taylor & Francis Group, London,
672 UK, 88, 2007.

673 Haitjema, H., Kuzin, S., Kelson, V., and Abrams, D.: Modeling flow into horizontal wells in a
674 Dupuit-Forchheimer model, *Ground Water*, 48(6), 878–883, doi:10.1111/j.1745-
675 6584.2010.00694.x, 2010.

676 Hantush, M. S. and Papadopoulos, I. S.: Flow of groundwater to collector wells, *J. Hydr. Eng.
677 Div.*, 88(5), 221–244, 1962.

678 Huang, C. S., Chen, Y. L., and Yeh, H. D.: A general analytical solution for flow to a single
679 horizontal well by Fourier and Laplace transforms, *Adv. Water Resour.*, 34(5), 640–648,
680 doi:10.1016/j.advwatres.2011.02.015, 2011.

681 Huang, C. S., Tsou, P. R., and Yeh, H. D.: An analytical solution for a radial collector well
682 near a stream with a low-permeability streambed, *J. Hydrol.*, 446, 48–58,
683 doi:10.1016/j.jhydrol.2012.04.028, 2012.

684 Huang, C. S., Lin, W. S., and Yeh, H. D.: Stream filtration induced by pumping in a confined,

685 unconfined or leaky aquifer bounded by two parallel streams or by a stream and an
686 impervious stratum, *J. Hydrol.*, 513, 28–44, doi:10.1016/j.jhydrol.2014.03.039, 2014.

687 Hunt, B.: Unsteady stream depletion from ground water pumping, *Ground Water*, 37(1),
688 98–102, doi:10.1111/j.1745-6584.1999.tb00962.x, 1999.

689 Hunt, B.: Flow to vertical and nonvertical wells in leaky aquifers, *J. Hydrol. Eng.*, 10(6),
690 477–484, doi:10.1061/(ASCE)1084-0699(2005)10:6(477), 2005.

691 Jasperse, J.: Planning, design and operations of collector 6, Sonoma County Water Agency,
692 NATO Sci. Peace Secur., 169–202, doi:10.1007/978-94-007-0026-0_11, 2009.

693 Kawecki, M. W.: Transient flow to a horizontal water well, *Ground Water*, 38(6), 842–850,
694 doi:10.1111/j.1745-6584.2000.tb00682.x, 2000.

695 Kawecki, M. W. and Al-Subaikhy, H. N.: Unconfined linear flow to a horizontal well, *Ground*
696 *Water*, 43(4), 606–610, doi:10.1111/j.1745-6584.2005.0059.x, 2005.

697 Kompani-Zare, M., Zhan, H., and Samani, N.: Analytical study of capture zone of a horizontal
698 well in a confined aquifer, *J. Hydrol.*, 307, 48–59, doi:10.1016/j.jhydrol.2004.09.021,
699 2005.

700 Kreyszig, E.: *Advanced engineering mathematics*, John Wiley & Sons, New York, 258, 1999.

701 Latinopoulos, P.: Analytical solutions for periodic well recharge in rectangular aquifers with
702 third-kind boundary conditions, *J. Hydrol.*, 77(1), 293–306, 1985.

703 Lee, E., Hyun, Y., Lee, K. K., and Shin, J.: Hydraulic analysis of a radial collector well for
704 riverbank filtration near Nakdong River, South Korea, *Hydrogeol. J.*, 20(3), 575–589,
705 doi:10.1007/s10040-011-082-3, 2012.

706 Mohamed, A. and Rushton, K.: Horizontal wells in shallow aquifers: Field experiment and
707 numerical model, *J. Hydrol.*, 329(1–2), 98–109, doi:10.1016/j.jhydrol.2006.02.006, 2006.

708 Neuman, S. P.: Theory of flow in unconfined aquifers considering delayed response of the
709 water table, *Water Resour. Res.*, 8(4), 1031–1045, 1972.

710 Nyholm, T., Christensen, S., and Rasmussen, K. R.: Flow depletion in a small stream caused
711 by ground water abstraction from wells, *Ground Water*, 40(4), 425–437, 2002.

712 Park, E. and Zhan, H. B.: Hydraulics of a finite-diameter horizontal well with wellbore storage
713 and skin effect, *Adv. Water Resour.*, 25(4), 389–400, doi:10.1016/S0309-
714 1708(02)00011-8, 2002.

715 Park, E. and Zhan, H. B.: Hydraulics of horizontal wells in fractured shallow aquifer systems,
716 *J. Hydrol.*, 281(1–2), 147–158, doi:10.1016/S0022-1694(03)00206-3, 2003.

717 Rodriguez, L., Vives, L., and Gomez, A.: Conceptual and numerical modeling approach of the
718 Guarani Aquifer System, *Hydrol. Earth Syst. Sci.*, 17, 295–314, doi:10.5194/hess-17-295-
719 2013, 2013.

720 Rushton, K. R. and Brassington, F. C.: Significance of hydraulic head gradients within
721 horizontal wells in unconfined aquifers of limited saturated thickness, *J. Hydrol.*, 492,
722 281–289, doi:10.1016/j.jhydrol.2013.04.006, 2013a.

723 Rushton, K. R. and Brassington, F. C.: Hydraulic behavior and regional impact of a horizontal
724 well in a shallow aquifer: example from the Sefton Coast, northwest England (UK),
725 *Hydrogeol. J.*, 21(5), 1117–1128, doi:10.1007/s10040-013-0985-0, 2013b.

726 Schafer, D. C.: Use of aquifer testing and groundwater modeling to evaluate aquifer/river
727 hydraulics at Louisville Water Company, Louisville, Kentucky, USA, *NATO Sci. Ser. IV*
728 *Earth Environ. Sci.*, 60, 179–198, doi:10.1007/978-1-4020-3938-6_8, 2006.

729 Steward, D. R.: Three-dimensional analysis of the capture of contaminated leachate by fully
730 penetrating, partially penetrating, and horizontal wells, *Water Resour. Res.*, 35(2),
731 461–468, doi:10.1029/1998WR900022, 1999.

732 Su, G. W., Jasperse, J., Seymour, D., Constantz, J., and Zhou, Q.: Analysis of pumping-induced
733 unsaturated regions beneath a perennial river, *Water Resour. Res.*, 43(8), W08421,
734 doi:10.1029/2006WR005389, 2007.

735 Sun, D. M. and Zhan, H. B.: Flow to a horizontal well in an aquitard-aquifer system, *J. Hydrol.*,
736 321(1–4), 364–376, doi:10.1016/j.jhydrol.2005.08.008, 2006.

737 Sun, D. M. and Zhan, H. B.: Pumping induced depletion from two streams, *Adv. Water Resour.*,
738 30, 1016–1026, doi:10.1016/j.advwatres.2006.09.001, 2007.

739 Todd, D. K. and Mays, L. W.: *Groundwater hydrology*, John Wiley & Sons, Inc., New Jersey,
740 USA, 240, 2005.

741 Tsou, P. R., Feng, Z. Y., Yeh, H. D., and Huang, C. S.: Stream depletion rate with horizontal
742 or slanted wells in confined aquifers near a stream, *Hydrol. Earth Syst. Sc.*, 14(8),
743 1477–1485, doi:10.5194/hess-14-1477-2010, 2010.

744 Unland, N. P., Cartwright, I., Cendón, D. I., and Chisari, R.: Residence times and mixing of
745 water in river banks: implications for recharge and groundwater–surface water exchange,
746 *Hydrol. Earth Syst. Sc.*, 18, 5109–5124, doi:10.5194/hess-18-5109-2014, 2014.

747 Wang, C. T. and Yeh, H. D.: Obtaining the steady-state drawdown solutions of constant-head
748 and constant-flux tests, *Hydrol. Process.*, 22(17), 3456–3461, doi:10.1002/hyp.6950,
749 2008.

750 Yeh, H. D., Chang, Y. C., and Zlotnik, V. A.: Stream depletion rate and volume from
751 groundwater pumping in wedge-shaped aquifers, *J. Hydrol.*, 349(3–4), 501–511,
752 doi:10.1016/j.jhydrol.2007.11.025, 2008.

753 Yeh, H. D. and Chang, Y. C.: Recent advances in modeling of well hydraulics, *Adv. Water*
754 *Resour.*, 51, 27–51, doi:10.1016/j.advwatres.2012.03.006, 2013.

755 Yeh, H. D., Huang, C. S., Chang, Y. C., and Jeng, D. S.: An analytical solution for tidal
756 fluctuations in unconfined aquifers with a vertical beach, *Water Resour. Res.*, 46, W10535,
757 doi:10.1029/2009WR008746, 2010.

758 Zhan, H. B. and Zlotnik, V. A.: Groundwater flow to a horizontal or slanted well in an
759 unconfined aquifer, *Water Resour. Res.*, 38(7), doi:10.1029/2001WR000401, 2002.

760 Zhan, H. B. and Park, E.: Horizontal well hydraulics in leaky aquifers, *J. Hydrol.*, 281(1–2),
761 129–146, doi:10.1016/S0022-1694(03)00205-1, 2003.

762 Zhan, H. B., Wang, L. V., and Park, E.: On the horizontal-well pumping tests in anisotropic
763 confined aquifers, *J. Hydrol.*, 252(1–4), 37–50, doi:10.1016/S0022-1694(01)00453-X,
764 2001.

765 Zheng, C. and Bennett, G. D.: *Applied contaminant transport modeling*, 2nd ed., Wiley-
766 Interscience, N.Y., 287, 2002.

767 Zhou, Y., Wenninger, J., Yang, Z., Yin, L., Huang, J., Hou, L., Wang, X., Zhang, D., and
768 Uhlenbrook, S.: Groundwater–surface water interactions, vegetation dependencies and
769 implications for water resources management in the semi-arid Hailiutu River catchment,
770 China – a synthesis, *Hydrol. Earth Syst. Sci.*, 17, 2435–2447, doi:10.5194/hess-17-2435-
771 2013, 2013.

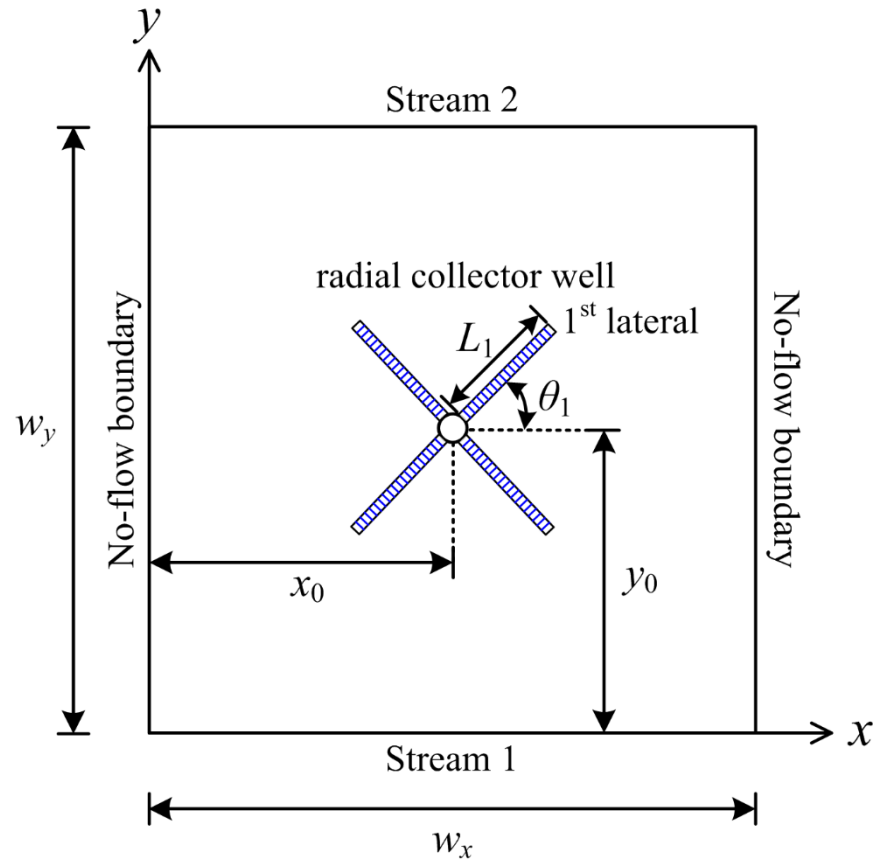
772 Zlotnik, V. A.: A concept of maximum stream depletion rate for leaky aquifers in alluvial
773 valleys, *Water Resour. Res.*, 40(6), W06507, doi:10.1029/2003WR002932, 2004.

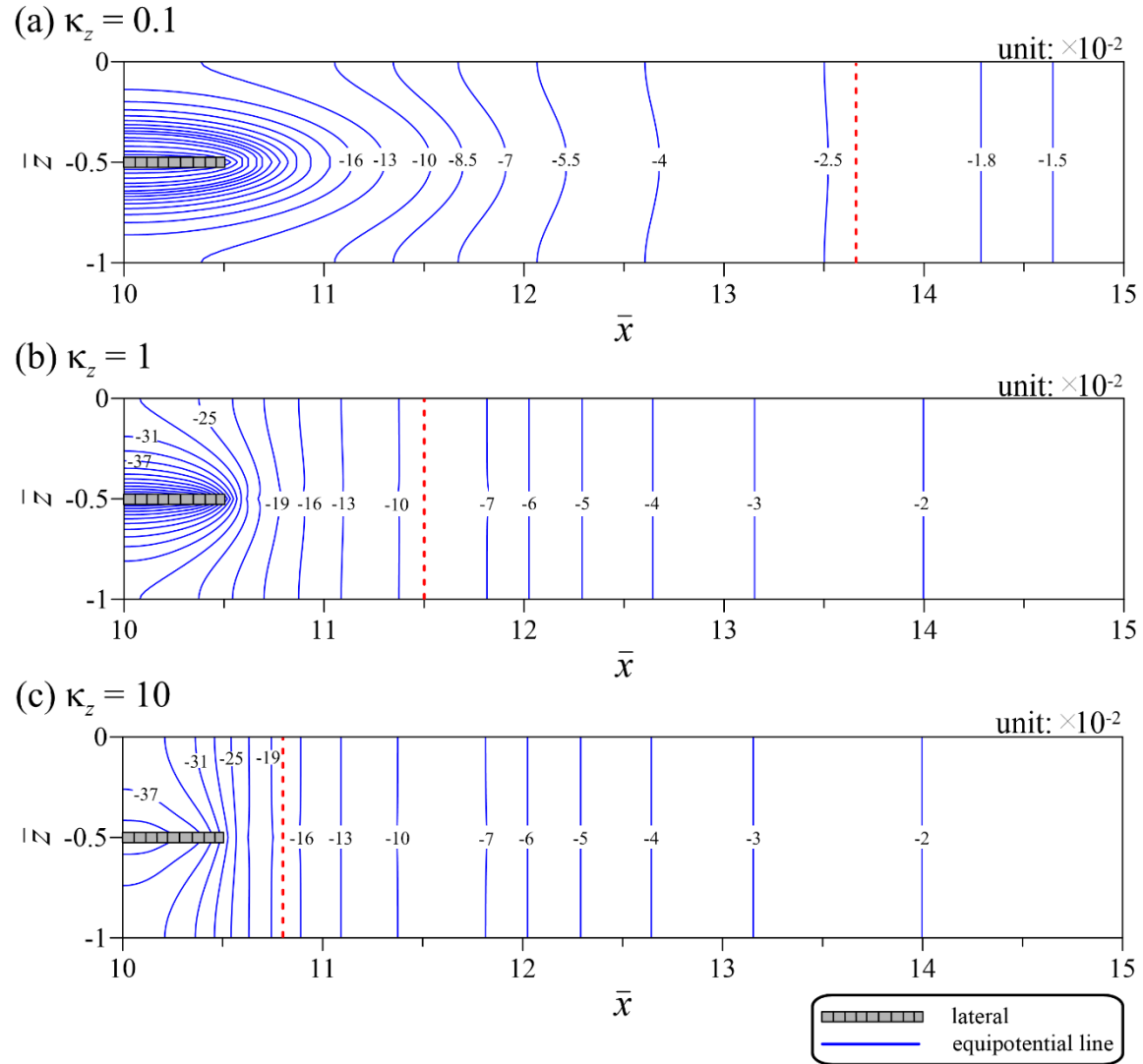
774 **Table 1.** Symbols used in the text and their definitions.

Symbol	Definition
a	Shortest horizontal distance between stream 1 and the far end of lateral
\bar{a}	a/y_0
b_1, b_2	Thicknesses of streambeds 1 and 2, respectively
d	Shortest horizontal distance between the far end of lateral and location of having only horizontal flow
\bar{d}	d/y_0
H	Aquifer thickness
h	Hydraulic head
\bar{h}	$(K_y H h)/Q$
K_x, K_y, K_z	Aquifer hydraulic conductivities in x , y and z directions, respectively
(K_1, K_2)	Hydraulic conductivities of streambeds 1 and 2, respectively
L_k	Length of k -th lateral where $k \in (1, 2, \dots, N)$
\bar{L}_k	L_k/y_0
N	The number of laterals
Q	Pumping rate of point sink or radial collector well
p	Laplace parameter
p_i	$-\kappa_z \lambda_i^2 - \kappa_x \alpha_m^2 - \beta_n^2$
p'_i	$-\kappa_z \lambda_i^2 - \beta_n^2$
p_0	$\kappa_z \lambda_0^2 - \kappa_x \alpha_m^2 - \beta_n^2$
p'_0	$\kappa_z \lambda_0^2 - \beta_n^2$
R	Shortest horizontal distance between the far end of lateral and aquifer lateral boundary
S_s, S_y	Specific storage and specific yield, respectively
t	Time since pumping
\bar{t}	$(K_y t)/(S_s y_0^2)$
w_x, w_y	Aquifer widths in x and y directions, respectively
\bar{w}_x, \bar{w}_y	$w_x/y_0, w_y/y_0$
X_n	Equaling $X_{m,n}$ defined in Eq. (39) with $\alpha_m = 0$
$X_{n,k}$	Defined in Eq. (45)
x, y, z	Cartesian coordinate system
$\bar{x}, \bar{y}, \bar{z}$	$x/y_0, y/y_0, z/H$
\bar{x}_k	Coordinate \bar{x} of the far end of the k -th lateral

x_0, y_0, z_0	Location of center of RCW
$\bar{x}_0, \bar{y}_0, \bar{z}_0$	$x_0/y_0, 1, z_0/H$
x'_0, y'_0, z'_0	Location of point sink
$\bar{x}'_0, \bar{y}'_0, \bar{z}'_0$	$x'_0/y_0, y'_0/y_0, z'_0/H$
α_m	$m \pi / \bar{w}_x$
β_n	Roots of Eq. (19)
ϕ_n	Equaling $\phi_{m,n}$ defined in Eq. (32) with $\alpha_m = 0$
γ	$S_y / (S_s H)$
κ_x, κ_z	$K_x / K_y, (K_z y_0^2) / (K_y H^2)$
κ_1, κ_2	$(K_1 y_0) / (K_y b_1), (K_2 y_0) / (K_y b_2)$
λ_0, λ_i	Roots of Eqs. (40) and (41), respectively
λ_s, λ'_s	$\sqrt{(\kappa_x \alpha_m^2 + \beta_n^2) / \kappa_z}, \beta_n / \sqrt{\kappa_z}$
$\mu_{n,0}$	Equaling $\mu_{m,n,0}$ defined in Eq. (36) with $\alpha_m = 0$
$\nu_{n,i}$	Equaling $\nu_{m,n,i}$ defined in Eq. (37) with $\alpha_m = 0$
θ_k	Counterclockwise angle from x axis to k -th lateral where $k \in (1, 2, \dots, N)$
$\max \bar{x}_k, \min \bar{x}_k$	Maximum and minimum of \bar{x}_k , respectively, where $k \in (1, 2, \dots, N)$

Figures

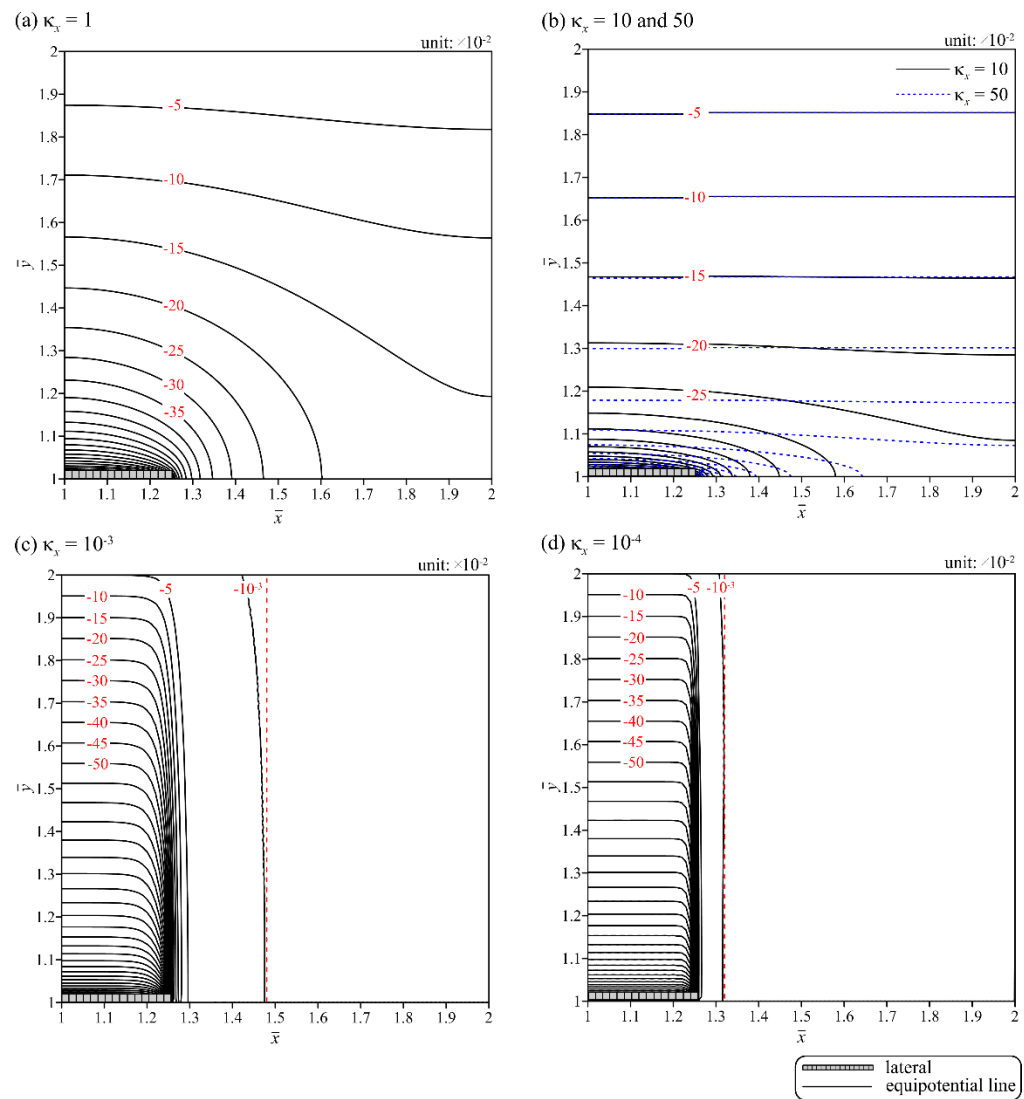




779

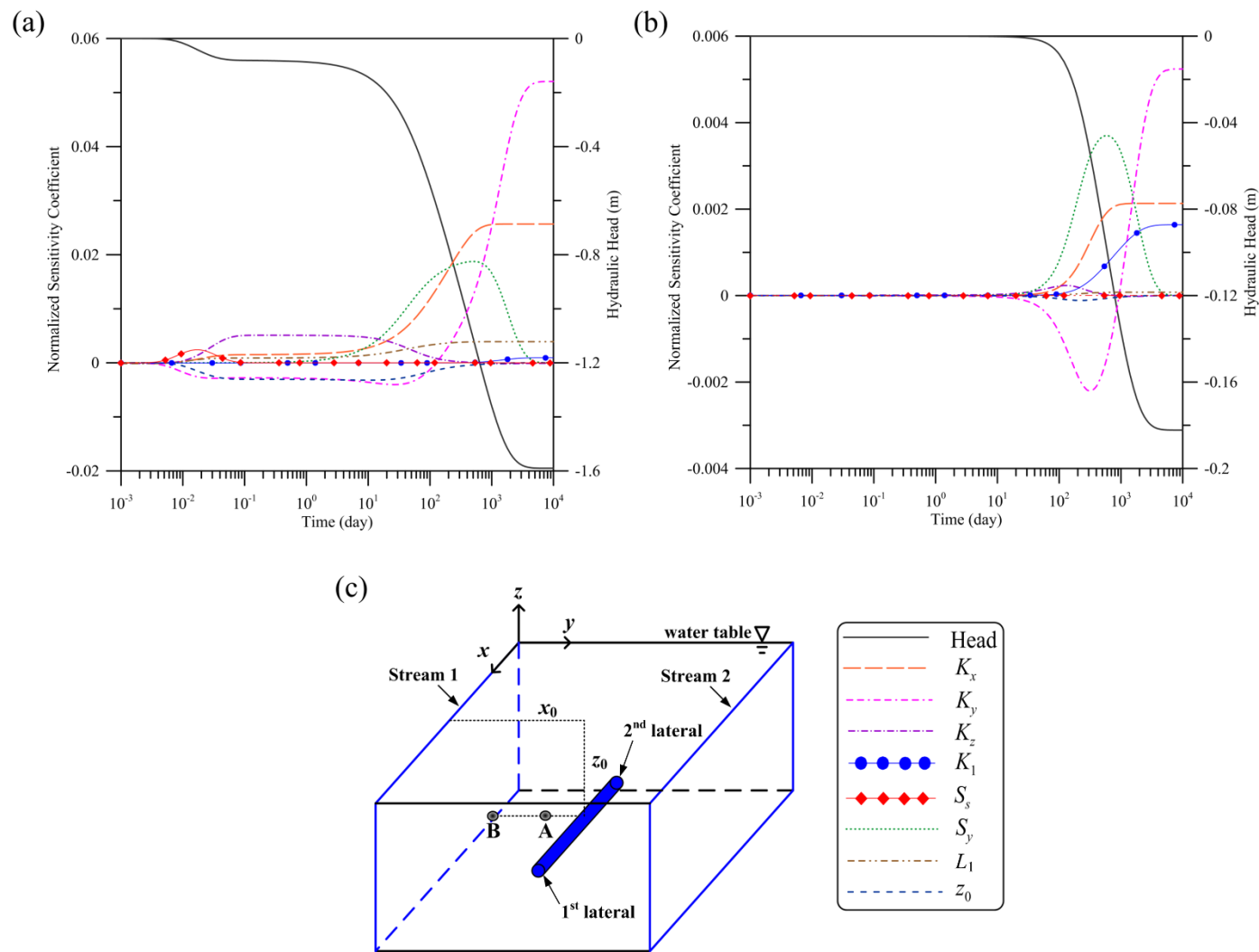
780

Figure 2. Equipotential lines predicted by the present solution for $\kappa_z =$ (a) 0.1, (b) 1 and (c) 10.



781

782 **Figure 3.** Spatial distributions of the dimensionless head predicted by the present head solution for $\kappa_x =$ (a) 1, (b) 10 and 50, (c) 10^{-3} and (d) 10^{-4} .

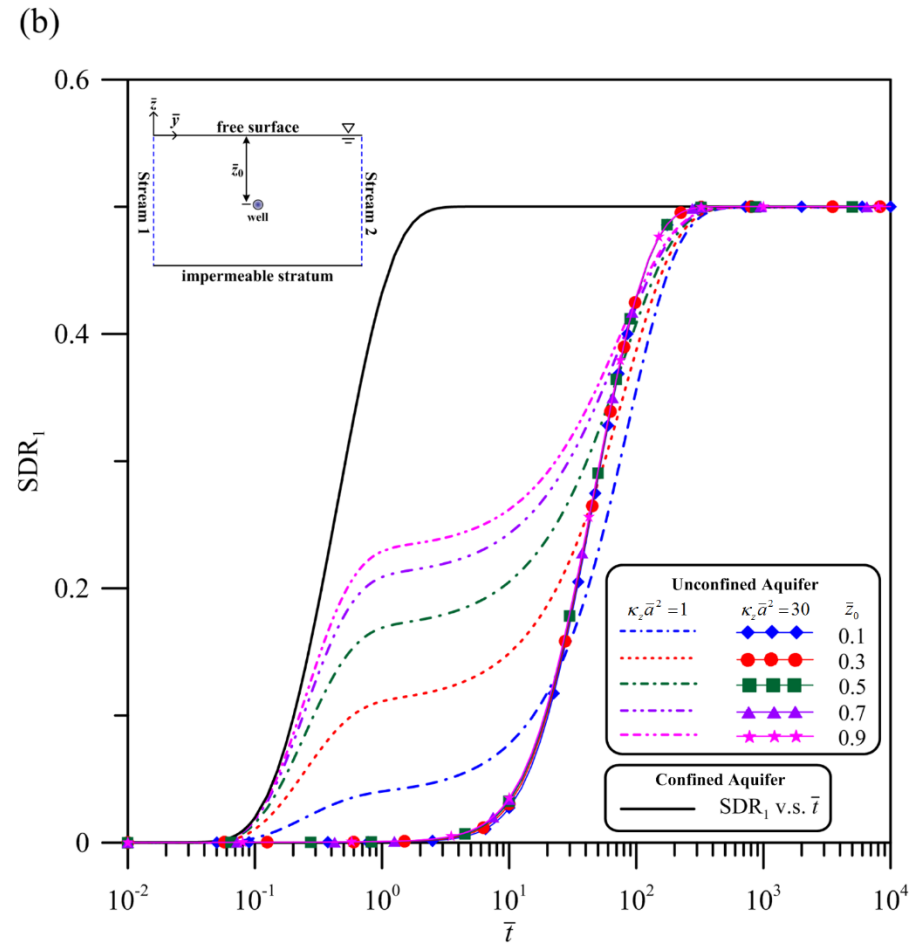
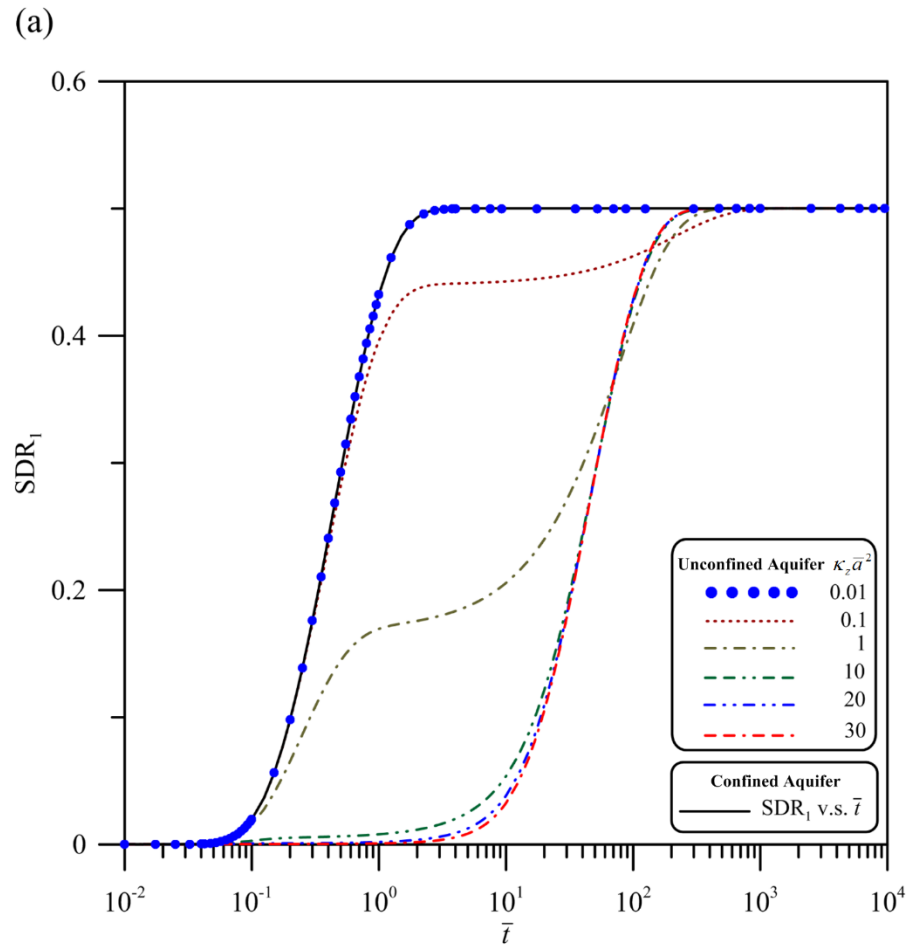


783

784

785

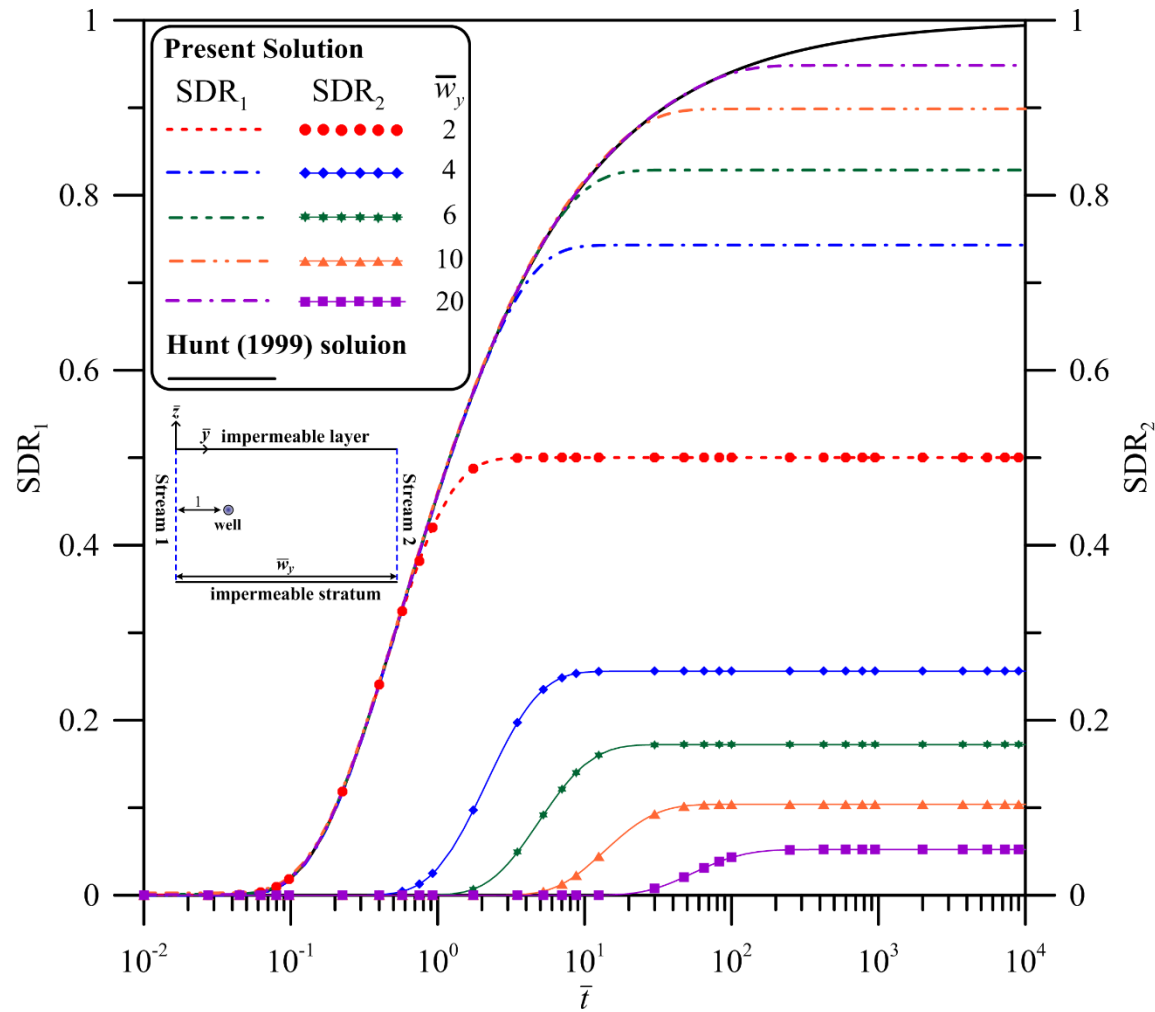
Figure 4. Temporal distribution curves of the normalized sensitivity coefficients for parameters K_x , K_y , K_z , S_s , S_y , K_1 , L_1 and z_0 observed at piezometers (a) A of (400 m, 340 m, -10 m) and (b) B of (400 m, 80 m, -10 m).



786

787

Figure 5. Temporal SDR₁ distributions predicted by Eq. (52) for stream 1 with various values of (a) $\kappa_z \bar{a}^2$ and (b) \bar{z}_0 .



788

789

Figure 6. Temporal SDR distribution curves predicted by Eqs. (52) and (53) with $\gamma = 0$ for confined aquifers when $\bar{w}_y = 2, 4, 6, 10$ and 20 .